BAROTROPIC INSTABILITY IN THE INNER CORE OF TROPICAL CYCLONES

by

James P. Edwards

Colorado State University

DEPARTMENT OF ATMOSPHERIC SCIENCE

PAPER NO. 552

BAROTROPIC INSTABILITY IN THE INNER CORE OF TROPICAL CYCLONES

by

James P. Edwards

Research supported by the

Office of Naval Research

under Grant number N000014-88-K-0214

Department of Atmospheric Science

Colorado State University

Fort Collins, Colorado

Spring 1994

Atmospheric Science Paper No. 552

ABSTRACT

BAROTROPIC INSTABILITY IN THE INNER CORE OF TROPICAL CYCLONES

The theory of barotropic stability of a vortex is presented including Rayleigh's condition, Fjørtoft's condition, Ripa's Theorem and Arnol'd's Theorem. The probable profile of potential vorticity (PV) in a tropical cyclone is discussed. It is likely that this profile has at least one reversal of the radial gradient of PV in the inner region of the storm. This reversal of PV gradient is a necessary condition for barotropic instability.

Linear normal mode analysis of many tangential wind profiles from the data set of Gray and Shea (1976) indicate that barotropic instability may be a common feature of mature tropical cyclones. The modified Rankine profile, the Holland (1980) profile and two profiles developed in this paper are also analyzed. Results indicate that a single reversal of vorticity gradient over the entire radial extent of the storm may produce low wavenumber instability while more localized reversals tend toward higher wavenumber instability. These instabilities have e-folding times on the order of a few hours and are generally located in the vicinity of the PV gradient reversal which is typically just within the radius of maximum winds. These results lead us to conclude that barotropic instability may be the primary cause of the polygonal eye walls which are observed in many tropical cyclones.

ACKNOWLEDGEMENTS

Thanks to my advisor Dr. Wayne S. Schubert, to my committee members Dr. Michael T. Montgomery, Dr. David A. Randall, and Dr. Gerald D. Taylor. Thanks also to Lígia Ribeiro Bernardet, Paul E. Ciesielski, Dr. Chungu Lu, Rosana Nieto Ferreira, Richard K. Taft, and Gerald B. Smith II each of whom has made a unique contribution to this work. Discussions with all of these people (and many others I have run into in the hall but failed to mention here) have been indispensable in the completion of this work. Special mention should go to Drs. Schubert and Montgomery both of whom have provided a depth of knowledge beyond that which is available in any text.

This work has been supported by the Office of Naval Research under Grant N000014-88-K-0214.

PREFACE

We are pleased to announce that at the time of publication this document is also available on the internet via hypertext transfer protocol (HTTP) at the Colorado State University Department of Atmospheric Science server
http://eclipse.atmos.colostate.edu/html/jimthesis/jim.html
This technology is an exciting new opportunity for scientists around the world to communicate ideas to each other and to the larger community. As new technology, however, it is subject to changes at any time. In particular the server address may be changed in the near future.

Questions or comments regarding this work can be directed to the author via e-mail at *jims@fermi.atmos.colostate.edu.*

CONTENTS

LIST OF FIGURES

LIST OF TABLES

Chapter 1

INTRODUCTION

The hurricane is one of the most studied of all tropospheric weather phenomena. Yet, low radar reflectivity within the eyewall, high wind speeds and relatively small spatial scale continue to make the inner core (defined here as the inner 1° radius of the storm) of the hurricane one of the least understood tropospheric weather features. One identifying feature of almost all hurricanes is the eye, a roughly circular area of relative calm surrounded by the storm. The eyewall is a cloud wall of intense convection located just within the radius of maximum winds. A recent study of hurricane Gloria (1985) by Franklin et al. (1993) is based on one of the most extensive data sets ever compiled for a single storm, yet no reliable data could be gathered within 13 km of the storm center. When one considers that this storm had a radius of maximum winds of only 19 km it is clear that there remains a significant gap in our understanding of the dynamics of tropical cyclones.

The shape of the eyewall, as mentioned above, is nearly circular. Yet, often this wall is observed by radar and satellite to contain some straight line configurations and/or takes on the appearance of a polygon of low order (e.g. triangle, rectangle, pentagon). Lewis and Hawkins (1982) present observations of several Atlantic basin storms which form polygonal eyewalls including this radar image of hurricane Betsy (1965) (Figure 1.1). Muramatsu (1986) reported observations of several storms including typhoon WYNNE (1980) which presented several different eyewall shapes (square, pentagon, and hexagon) at various times (Figure 1.2). Black and Marks (1991) noted a meso-vortex, which we believe to be a related feature, within the eye of hurricane Hugo (1989), during a rather dramatic flight in which an engine loss caused them to orbit inside the eye for over an hour in order to regain sufficient altitude to escape the storm.

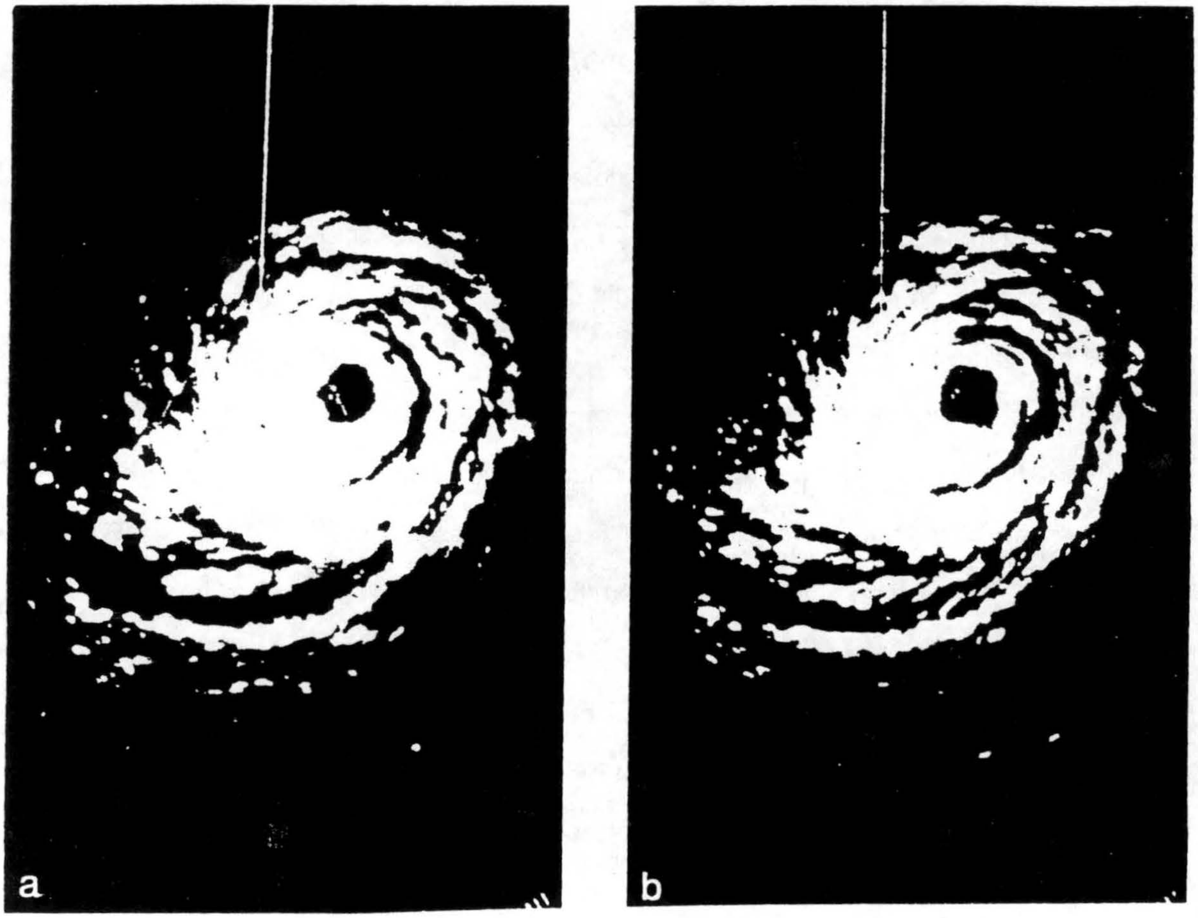

Figure 1.1: Two examples of polygonal features observed by the Key West, Fl., WSR-57 radar in Hurricane Betsy (1965): a) hexagonal eye at 0748 GMT on 8 September 1965 and b) square eye at 0803. (From Lewis and Hawkins (1982))

Lewis and Hawkins gave an explanation for the formation of these polygonal eyes based on the superposition of horizontally propagating gravity waves. Muramatsu dismissed this explanation since the observed structures seem confined to a narrow region near the eyewall and, barring the possibility of some kind of wave guide effect, there is no reason that gravity waves should be restricted to that area. Muramatsu further noted that these features are quite similar to features found in tornadoes and presented in theoretical studies by Snow (1978) and Staley and Gall (1979).

Rotunno (1986) and Snow (1982) provide further discussion of tornado dynamics and tornadogenesis. The tornado vortex is observed to form within a larger tornado cyclone and in many cases several vortices are observed within the same cyclone. This multiple vortex phenomenon is also observed in vortex chamber experiments in which the swirl ratio, the ratio of circulation to flow volume through the chamber, is large. Each of the authors also suggest that barotropic instability, although not providing a complete explanation, may play a roll in tornado dynamics.

The papers discussed above are the only papers regarding polygonal eyes to appear in the refereed literature. This suggests that these features may be considered a novelty and unimportant in light of the problems of determining storm track and strength. However, we will argue here that polygonal eyewall features are an indication of the most basic dynamic structure of the storm, a structure which may indeed be quite important in determining both the strength and the track of the hurricane. We will show that barotropic instability may be a regularly occurring feature of tropical cyclones, and that this barotropic instability may often result in the formation of polygonal eyewalls. To this end we will consider the two dimensional linear dynamics of a hydrostatic vortex with no friction and no forcing. These dynamics are well represented by the shallow water model which has a long history of use in this type of study, most likely beginning with Lords Rayleigh and Kelvin late in the nineteenth century.

It is well accepted that, in this context, the hurricane can be considered as consisting of an axisymmetric tangential wind with perturbations which cause radial flow and tangential deviations from symmetry. With these assumptions the question left to be asked is that

Figure 1.2: Hexagonal eye of typhoon WYNNE (1980) at 0400 GMT on October 12, 1980, by the Miyakojima radar. (From Muramatsu (1986))

of the structure of this basic state tangential wind or the related structure of the basic state potential vorticity. Two types of instability may occur as a result of this structure.

The first is inertial instability which results from a sufficient decrease of absolute angular momentum with increasing radius. For the inviscid axisymmetric case, given that the basic state velocity is everywhere positive, inertial instability requires

$$\frac{\partial(r\bar{v})}{r\partial r} < -f$$

in the northern hemisphere. The inner core of a tropical cyclone is generally observed to be a region of increasing absolute angular momentum so that inertial instability is highly unlikely there (Shea, 1972; Shapiro and Montgomery, 1993; Franklin et al. 1993). It may however be an important process in the upper tropospheric outflow region (Flatau and Stevens, 1989; 1993). A review of the theory of inertial stability can be found in Emanuel (1979).

The second is barotropic instability which results from a sufficiently large radial shear of the tangential wind. In Chapter 2 we will consider in detail the conditions for which barotropic instability may occur. In Chapter 3 we will use the model developed in Appendix A to determine the magnitude of instability growth for various profiles of tangential wind including those observed in the extensive data set of Shea (1972) as well as several idealized profiles which are developed in Appendix B.

It needs to be noted that the terms "hurricane" and "tropical cyclone" are used interchangeably throughout the text. The term "hurricane" is not intended to refer to a particular basin of formation, unless we refer to a specific named storm.

Chapter 2

THEORY OF BAROTROPIC STABILITY OF A HURRICANE VORTEX

For quasi-static frictionless, axisymmetric flow with diabatic sources, the Ertel potential vorticity equation is $DP/Dt = P\partial\dot{\theta}/\partial\theta$, where $P = (f + \zeta_\theta)/\sigma$ is the potential vorticity, $\zeta_\theta = \partial(rv)/r\partial r$ the isentropic relative vorticity (with v the tangential wind), $\sigma = -\partial p/\partial\theta$ the pseudodensity in θ-space, D/Dt the substantial derivative, and $\partial/\partial\theta$ the partial derivative with respect to θ but with absolute angular momentum held fixed (i.e. the derivative along the absolute vorticity vector). In a hurricane, the diabatic heat source $\dot{\theta}$ is primarily due to latent heat release, which tends to be a maximum in the midtroposphere of the moist convective region. Thus, the right hand side of the PV equation takes on large positive values in the lower troposphere at the radius of intense eye wall convection. Further, subsidence at the center of the eye would tend to bring upper tropospheric low PV air down to lower levels. These processes would combine to result in potential and relative vorticity fields which have maxima near the eye wall rather than at the hurricane center. Möller and Smith (1994) performed computations using a numerical model based on Schubert and Alworth (1987) in which the heating profile is maximum in an annular region of the middle trophosphere. Figure 2.1 shows their initial heating profile and the resulting nondimensional potential vorticity profile 48 hours later. The potential vorticity is defined here as $q/f = \zeta\sigma_0/(f\sigma)$ where σ_0 is a constant reference pseudo-density and σ is the pseudo-density in θ-space (see Schubert and Alworth 1987 for further details). These plots are in a potential radius coordinate system defined by $fR^2 = fr^2 + 2vr$.

The reversal of the radial gradient of potential vorticity at lower tropospheric levels in the hurricane sets the stage for combined barotropic-baroclinic instability. Since the potential vorticity field in the hurricane is induced by moist physical processes, we would

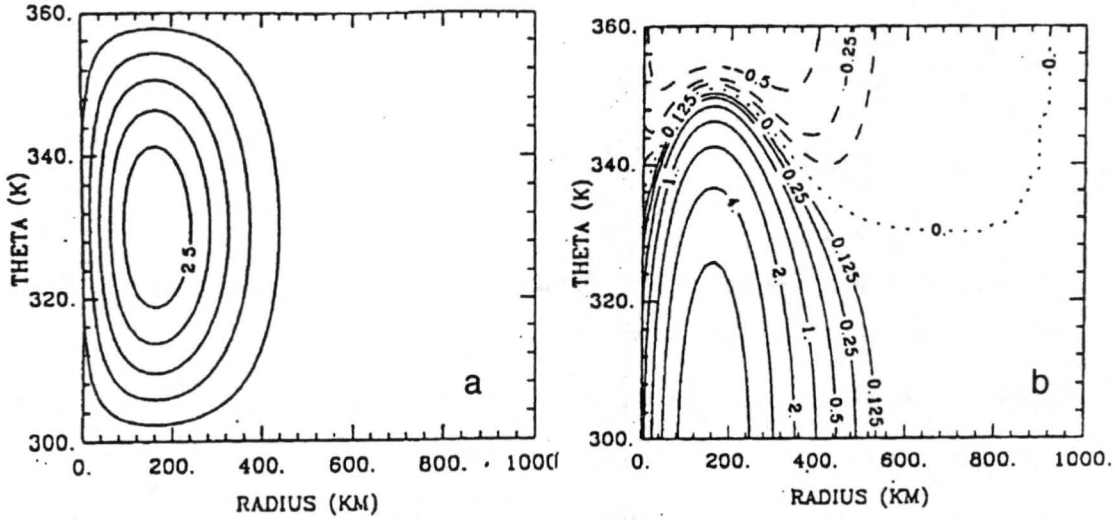

Figure 2.1: (a) The initial heating profile in degrees K per day and (b) the nondimensional potential vorticity profile q/f 48 hours later in isentropic - potential radius space from the model calculations of Möller and Smith (1994).

expect these same moist processes, along with barotropic and baroclinic instability effects, to play a role in the evolution of wave disturbances developing out of this background state. Apparently, barotropic processes play a particularly important role.

Here we will present a review of the theory of barotropic instability in a vortex. We begin with a consideration of the stability conditions for the linear nondivergent barotropic model, we then discuss the divergent case and finally the extension to the nondivergent nonlinear case. To our knowledge this represents the complete theory of barotropic instability for a vortex as it is understood today.

2.1 Nondivergent linear stability

Let us first consider the f-plane nondivergent barotropic vorticity equation linearized about a basic state tangential flow $\bar{v}$ which varies with radius. This equation takes the form

$$\frac{\partial \zeta'}{\partial t} + u'\frac{d\bar{\zeta}}{dr} + \bar{v}\frac{\partial \zeta'}{r\partial \phi} = 0, \tag{2.1}$$

where

$$\bar{\zeta} = f + \frac{\partial (r\bar{v})}{r\partial r} \tag{2.2}$$

$$\zeta' = \frac{\partial(rv')}{r\partial r} - \frac{\partial u'}{r\partial \phi}, \tag{2.3}$$

and the perturbation wind components (u', v') satisfy the nondivergent relation

$$\frac{\partial(ru')}{r\partial r} + \frac{\partial v'}{r\partial \phi} = 0. \tag{2.4}$$

We can express equation (2.1) in terms of a streamfunction, $\psi(r, \phi, t)$, defined such that

$$(u, v) = \left(-\frac{\partial \psi}{r\partial \phi}, \frac{\partial \psi}{\partial r}\right). \tag{2.5}$$

We now assume a waveform solution, $\psi(r, \phi, t) = \Psi(r) \exp(i(m\phi - \nu t))$, where m is the tangential wavenumber and must be an integer to insure continuity, and ν is the complex frequency of the wave. Thus equation (2.1) becomes

$$\left(\bar{v} - \frac{r\nu}{m}\right)\left[\frac{d}{rdr} r\frac{d\Psi}{dr} - \frac{m^2}{r^2}\Psi\right] - \Psi\frac{d\bar{\zeta}}{dr} = 0. \tag{2.6}$$

2.1.1 Rayleigh's condition and Fjørtoft's theorem

We now multiply equation (2.6) by $r\Psi^*/(\bar{v} - r\nu/m)$, where Ψ^* is defined as the complex conjugate of Ψ. Assuming that the perturbation streamfunction vanishes at the origin and at arbitrarily large r and integrating results in:

$$\int_0^\infty \left(\frac{m^2}{r}|\Psi|^2 + r\left|\frac{d\Psi}{dr}\right|^2 + \frac{r|\Psi|^2}{\left(\bar{v} - \frac{r\nu}{m}\right)}\frac{d\bar{\zeta}}{dr}\right) dr = 0. \tag{2.7}$$

Separating equation (2.7) into real and imaginary parts results in

$$\int_0^\infty \left(\frac{m^2}{r}|\Psi|^2 + r\left|\frac{d\Psi}{dr}\right|^2 + \frac{r|\Psi|^2(\bar{v} - r\nu_r/m)}{|\bar{v} - r\nu/m|^2}\frac{d\bar{\zeta}}{dr}\right) dr = 0, \tag{2.8}$$

$$\frac{\nu_i}{m}\int_0^\infty \frac{r^2|\Psi|^2}{|\bar{v} - r\nu/m|^2}\frac{d\bar{\zeta}}{dr}dr = 0. \tag{2.9}$$

From equation (2.9) we see that if $\nu_i \neq 0$ then $d\bar{\zeta}/dr$ must have both signs in the domain. That is, the gradient of the basic state vorticity with respect to radius must reverse itself. This is Rayleigh's necessary condition for instability. Another, more stringent, condition can be derived by considering equation (2.8). We again assume $\nu_i \neq 0$ but now we assume that Rayleigh's condition is satisfied and define r_s as the radius at which $d\bar{\zeta}/dr = 0$, and $\bar{\omega}_s = \bar{v}(r_s)/r_s$. From (2.9) we then get

$$\left(\frac{\nu_r}{m} - \bar{\omega}_s\right) \int_0^\infty \frac{r^2 |\Psi|^2}{|\bar{v} - r\nu/m|^2} \frac{d\bar{\zeta}}{dr} dr \quad = \quad 0. \tag{2.10}$$

Adding this to equation (2.8) results in

$$\int_0^\infty \frac{r^2 |\Psi|^2}{|\bar{v} - r\nu/m|^2} (\bar{\omega} - \bar{\omega}_s) \frac{d\bar{\zeta}}{dr} dr \quad = \quad - \int_0^\infty \left(\frac{m^2}{r} |\Psi|^2 + r \left| \frac{d\Psi}{dr} \right|^2 \right) dr \tag{2.11}$$

Since the right hand side of this equation must be less than zero, it follows that

$$(\bar{\omega} - \bar{\omega}_s) \frac{d\bar{\zeta}}{dr} \quad < \quad 0 \tag{2.12}$$

somewhere within the domain. This is Fjørtoft's (1950) theorem.

2.1.2 The semicircle theorem

A third theorem, known as Howard's semicircle theorem, provides an upper bound on the growth rate of instability, ν_i, for the normal mode linear problem, as well as an upper bound on the frequency of neutral normal modes. Here we will derive the theorem following Pedlosky (1970). Later in chapter 4 we will examine the usefulness of this upper bound in predicting normal mode growth rates.

We now define $W = \bar{v} - r\nu/m$, and F such that $\Psi = FW$. Equation (2.6) can then be written

$$\frac{d}{rdr} \left(rW^2 \frac{dF}{dr} \right) - (m^2 - 1) \frac{W^2 F}{r^2} \quad = \quad 0. \tag{2.13}$$

Multiplying this equation by rF^*, where F^* is the complex conjugate of F, and integrating over r results in

$$\int_0^\infty \left\{ F^* \frac{d}{dr} \left(rW^2 \frac{dF}{dr} \right) - (m^2 - 1) \frac{W^2 F F^*}{r} \right\} dr \quad = \quad 0, \tag{2.14}$$

which can be written as

$$\int_0^\infty W^2 Q r dr \quad = \quad 0, \tag{2.15}$$

where

$$Q = \left|\frac{dF}{dr}\right|^2 + \frac{m^2-1}{r^2}|F|^2. \tag{2.16}$$

If we first assume that ν is real valued we see from equation (2.15) that either $Q \equiv 0$, or that $W^2 = 0$ and thus F has a singularity somewhere in the domain. It can be shown that $Q \equiv 0$ is a trivial solution, and it is easy to see that if F has a singularity somewhere in the domain then $\bar{\omega}_{min} \leq \nu/m \leq \bar{\omega}_{max}$ which provides an upper bound on the frequency of normal mode rotation with respect to the basic state flow.

If we now assume that $\nu = \nu_r + i\nu_i$ where $\nu_i \neq 0$ we can find an upper bound on the growth rate (ν_i). Separating ν into real and imaginary parts gives

$$W^2 = \left(\bar{v} - \frac{r\nu_r}{m}\right)^2 - \left(\frac{r\nu_i}{m}\right)^2 - i2\frac{r\nu_i}{m}\left(\bar{v} - \frac{r\nu_r}{m}\right). \tag{2.17}$$

Using this we can separate equation (2.15) into real and imaginary parts

$$\int_0^\infty \left(\bar{v}^2 - \frac{2r\nu_r}{m}\bar{v} + (\frac{r\nu_r}{m})^2 - (\frac{r\nu_i}{m})^2\right) Qr\,dr = 0, \tag{2.18}$$

$$\nu_i \int_0^\infty \left(\bar{v} - \frac{r\nu_r}{m}\right) Qr^2 dr = 0. \tag{2.19}$$

From equation (2.19), assuming $\nu_i \neq 0$, we have

$$\frac{\nu_r}{m}\int_0^\infty Qr^3 dr = \int_0^\infty \bar{\omega} Q r^3 dr \tag{2.20}$$

where $\bar{\omega} = \bar{v}/r$ is the basic state angular velocity. Using

$$\int_0^\infty (\bar{\omega} - \bar{\omega}_{max})(\bar{\omega} - \bar{\omega}_{min}) Q r^3 dr \leq 0 \tag{2.21}$$

in equation (2.18) we have

$$\int_0^\infty \left[\left(\frac{2\nu_r}{m} - \bar{\omega}_{max} - \bar{\omega}_{min}\right)\bar{\omega} - \frac{\nu_r^2}{m^2} + \frac{\nu_i^2}{m^2} + \bar{\omega}_{min}\bar{\omega}_{max}\right] Qr^3 dr \leq 0. \tag{2.22}$$

We now combine this with equation (2.20) to get

$$\left[\frac{\nu_r}{m} - \frac{1}{2}(\bar{\omega}_{max} + \bar{\omega}_{min})\right]^2 + \left(\frac{\nu_i}{m}\right)^2 \leq \left[\frac{1}{2}(\bar{\omega}_{max} - \bar{\omega}_{min})\right]^2 \tag{2.23}$$

which shows that the growth rate of instability is bounded by the range of angular velocity in the system and the frequency of the mode. This can be represented by a semicircle in the (ν_r, ν_i) plane as shown in Figure 3.4 on page 25.

2.1.3 Algebraic stability

When the complete solution set for any linear problem is known, any solution to the problem can be written as a superposition, or sum, of members of this solution set. In shear flow problems, however, the set of normal mode solutions generally does not comprise a complete set of solutions. (e.g. Drazin and Reid 1981, pp 147-153). Case (1960) and others have shown that there are also algebraic solutions which are required to represent the solution subject to an arbitrary initial condition. To solve the initial value problem it is traditional to compute the Fourier transform with respect to ϕ and the Laplace transform with respect to t (e.g., Case 1960, Farrell 1987, Carr and Williams 1989). Thus, let

$$\psi_{sm}(r) = \int_0^\infty \int_0^{2\pi} \exp\left(-(st + im\phi)\right) \psi(\phi, r, t)\, d\phi\, dt, \tag{2.24}$$

where m is the Fourier tangential wavenumber, and s is the Laplace transform parameter. The joint Fourier - Laplace transform of equation (2.1) expressed in terms of the streamfunction ψ' gives

$$(s + im\bar{v}) \left(\frac{\partial}{r\partial r}\left[r\frac{\partial \psi_{sm}}{\partial r}\right]\right) + \left(-\frac{im}{r}\frac{\partial}{\partial r}\left[\frac{\partial(r\bar{v})}{r\partial r}\right] - \frac{m^2}{r^2}(s + im\bar{v})\right)\psi_{sm} \;=\; \nabla^2\psi_{0m}, \tag{2.25}$$

where ψ_{0m} is the m^{th} Fourier component of the initial streamfunction. Rearrangement of this equation gives

$$\left(\frac{\partial^2}{\partial r^2} + \frac{\partial}{r\partial r} - \frac{im}{r(s + im\bar{v})}\frac{\partial}{\partial r}\left(\frac{\partial r\bar{v}}{r\partial r}\right) - \frac{m^2}{r^2}\right)\psi_{sm} = \frac{\nabla^2\psi_{0m}}{s + im\bar{v}}. \tag{2.26}$$

Carr and Williams (1989) have solved equation (2.26) for the special case of a bounded annular region with the basic state tangential wind decreasing as $1/r$. (This choice of basic state renders the third term of equation (2.26) identically zero.) Smith (1994) generalized this work to include an inner vortex region with uniform vorticity as well as three regions of constant vorticity. We have recently extended his work to multiple regions in Appendix A. This model is shown to be the nonhomogeneous counterpart of the homogeneous system of differential equations represented by the eigensystem (A.21). We are aware of no closed form solutions of equation (2.26) for which the third term is not identically zero.

Algebraic solutions always decay given sufficient time. That is, in the limit as $t \to \infty$, the problem can always be represented in terms of exponential normal modes. However, they may grow faster than the exponential modes for a short time after certain "initial" conditions have been satisfied. We do not feel it is adequate to assume, as is often done in normal mode analysis, that a sufficient amount of time has passed since the "initial" time for two reasons.

First, there are always processes in nature which cannot be incorporated into any model. Any one or combination of these forces may serve to induce the "initial" condition necessary for algebraically unstable modes at any time.

Second, linear theory is only applicable in the limit of small deviations from the basic state. There is no reason to assume that the exponential normal modes should dominate the solution before this limit is reached, an algebraic mode may reach this limit itself before its eventual decay or it may serve to shift the exponential growth curve of a normal mode to the left thus affecting the nonlinear regime much sooner than the normal mode growth rate might suggest.

However, the solution of the swirling initial value problem for this system is often a formidable task and has only been solved analytically for certain very simple basic states (e.g. Carr and Williams 1989, Smith 1994). Therefore we will limit the scope of this paper to discussion of the discrete normal mode solutions with recognition that this is an important subset of the larger problem.

2.1.4 Rayleigh's condition

The possibility of existence of the continuous spectrum of algebraic solutions shows us that any theorem which relies on the assumption of waveform solutions in time may not be applicable to all solutions of the system. The semicircle theorem tells us something about the amplitude of the normal mode frequencies themselves and thus relies a priori on this form. However we can derive Rayleigh's condition without the use of normal modes and thus be insured that it applies to all solutions to the problem. The idea here (and in the following sections on Ripa's theorem and Arnol'd's theorem) is to form an equation consisting only of a time derivative and flux terms. This equation is then integrated over the domain, with the assumption that the flux terms are suitably well behaved to vanish under the integral. The resulting equation states that the function inside the time derivative must be constant in time over the domain. If we are fortuitous, we can then make a statement about the structure of a basic state which is (or is not) stable to perturbations.

We begin by forming a perturbation enstrophy equation from equation (2.1), where enstrophy is defined as the square of the vorticity,

$$\frac{\partial}{\partial t}\left(\tfrac{1}{2}\zeta'^2\right)+\bar{\omega}\frac{\partial}{\partial \phi}\left(\tfrac{1}{2}\zeta'^2\right)+u'\zeta'\frac{\partial\bar{\zeta}}{\partial r} \;=\; 0 \tag{2.27}$$

Then we use equation (2.3) in equation (2.27) and divide by $d\bar{\zeta}/rdr$ to get

$$\begin{aligned}&\frac{\partial}{\partial t}\left(\tfrac{1}{2}r\zeta'^2\left(\frac{d\bar{\zeta}}{dr}\right)^{-1}\right)+\frac{\partial\left(r^2u'v'\right)}{r\partial r}\;+\\ &\frac{\partial}{r\partial\phi}\left(\tfrac{1}{2}\bar{v}\zeta'^2r\left(\frac{d\bar{\zeta}}{dr}\right)^{-1}-\tfrac{1}{2}u'^2\right)\;-\;rv'\frac{\partial(ru')}{r\partial r}=0.\end{aligned} \tag{2.28}$$

Let us now define the wave-activity by

$$A(\bar{\zeta},\zeta') \;=\; r\left(-\frac{d\bar{\zeta}}{dr}\right)^{-1}\tfrac{1}{2}(\zeta')^2, \tag{2.29}$$

and use the continuity equation (2.4) to arrive at the wave activity relation

$$\frac{\partial A}{\partial t}+\frac{\partial\left[-r^2u'v'\right]}{r\partial r}+\frac{\partial\left[\bar{v}A-\tfrac{1}{2}r(v'^2-u'^2)\right]}{r\partial\phi} \;=\; 0. \tag{2.30}$$

Finally, integration of (2.30) over the domain yields

$$\frac{d}{dt}\iint A\,rdrd\phi \;=\; \frac{d}{dt}\iint r\left(-\frac{d\bar{\zeta}}{dr}\right)^{-1}\tfrac{1}{2}\zeta'^2\,rdrd\phi=0. \tag{2.31}$$

Since the integrals in (2.31) must be constant in time, if $\bar{\zeta}$ is a monotonically decreasing function of r, ζ'^2 cannot grow in an overall sense. Thus, a sufficient condition for stability is that $d\bar{\zeta}/dr$ have the same sign throughout the domain. This argument shows that the perturbation enstrophy cannot grow in a global sense. It does not rule out the possibility that perturbations grow at one radius at the expense of perturbations elsewhere in the domain. Nor does it eliminate the possibility that the perturbation energy might grow without disturbing the perturbation enstrophy.

The simple linear barotropic argument given above can be generalized in several ways. Baroclinic effects can be included in both the quasigeostrophic (Charney and Stern 1962) and semigeostrophic (Eliassen 1983, Magnusdottir and Schubert 1990, 1991) frameworks. In addition the analysis need not be limited to parallel shear flows (Andrews 1983) or even to linearized dynamics (Arnol'd 1965, 1966; Drazin and Reid 1981; McIntyre and Shepherd 1987; Shepherd 1988a,b, 1989, 1990). We shall now consider the extension to the linear divergent case.

2.2 Linear stability in a barotropic model - Ripa's theorem

The nondivergent barotropic stability theorems of the previous section can be generalized to the divergent barotropic model and to discretely layered (but not continuously stratified) primitive equation models (Ripa 1983, 1991). For the shallow water case we consider the linearized momentum and continuity,

$$\frac{\partial u'}{\partial t} + \bar{v}\frac{\partial u'}{r\partial\phi} - \left(f + \frac{2\bar{v}}{r}\right)v' + g\frac{\partial h'}{\partial r} = 0, \tag{2.32}$$

$$\frac{\partial v'}{\partial t} + u'\frac{\partial \bar{v}}{\partial r} + \bar{v}\frac{\partial v'}{r\partial\phi} + \left(f + \frac{\bar{v}}{r}\right)u' + g\frac{\partial h'}{r\partial\phi} = 0, \tag{2.33}$$

$$\frac{\partial h'}{\partial t} + u'\frac{\partial \bar{h}}{\partial r} + \bar{v}\frac{\partial h'}{r\partial\phi} + \bar{h}\left(\frac{\partial(ru')}{r\partial r} + \frac{\partial v'}{r\partial\phi}\right) = 0, \tag{2.34}$$

where the primes denote small perturbations about a purely tangential basic flow $\bar{v}(r)$, with associated depth $\bar{h}(r)$, satisfying gradient balance $(f + \bar{v}/r)\bar{v} = g\partial\bar{h}/\partial r$.

To derive Ripa's theorem we need to combine (2.32)–(2.34) into equations for the perturbation energy, momentum, and potential vorticity, i.e.,

$$E' = \tfrac{1}{2}\left[\bar{h}(u'^2 + v'^2) + 2\bar{v}v'h' + gh'^2\right], \tag{2.35}$$

$$M' = rv'h', \tag{2.36}$$

$$P' = \frac{1}{\bar{h}}\left(\frac{\partial(rv')}{r\partial r} - \frac{\partial u'}{r\partial\phi} - \bar{P}h'\right), \tag{2.37}$$

where $\bar{P} = \left[f + \partial(r\bar{v})/r\partial r\right]/\bar{h}$. To derive the equation for E' we form $(\bar{h}u')\cdot(2.32) + (\bar{h}v' + h'\bar{v})\cdot(2.33) + (\bar{v}v' + gh')\cdot(2.34)$ to obtain

$$\frac{\partial E'}{\partial t} - \bar{h}^2\bar{v}u'P' + \frac{\partial[(\bar{v}v' + gh')\bar{h}ru']}{r\partial r} + \frac{\partial[(\bar{v}v' + gh')(\bar{h}v' + h'\bar{v})]}{r\partial\phi} = 0. \tag{2.38}$$

To derive the equation for M' we form $(rh')\cdot(2.33)+(rv')\cdot(2.34)$ resulting in

$$\frac{\partial M'}{\partial t} - r\bar{h}^2 u'P' + \frac{\partial\left[r^2\bar{h}u'v'\right]}{r\partial r} + \frac{\partial\left[\bar{v}M' + \frac{1}{2}r\left(gh'^2 + \bar{h}(v'^2 - u'^2)\right)\right]}{r\partial\phi} = 0. \quad (2.39)$$

The equation for P', obtained by forming the vorticity equation from (2.32)−(2.33) and then eliminating the divergence using (2.34), takes the form

$$\frac{\mathcal{D}P'}{\mathcal{D}t} + \frac{d\bar{P}}{dr}u' = 0, \quad (2.40)$$

where $\mathcal{D}/\mathcal{D}t = \partial/\partial t + \bar{\omega}\partial/\partial\phi$. This is the divergent form of equation (2.1).

Defining the radial particle displacement η by $\mathcal{D}\eta/\mathcal{D}t = u'$, we can integrate (2.40) to obtain

$$P' + \frac{d\bar{P}}{dr}\eta = F(r) \quad (2.41)$$

where $F(r)$ is an arbitrary function of r. We restrict ourselves here to the case where $F(r)\equiv 0$ which may preclude applicability to certain problems similar in nature to that studied by Case (1960). Multiplication of (2.41) by u' yields

$$u'P' = -\frac{\mathcal{D}}{\mathcal{D}t}\left(\frac{d\bar{P}}{dr}\frac{1}{2}\eta^2\right) = -\frac{\mathcal{D}}{\mathcal{D}t}\left(\frac{1}{2}P'^2\left(\frac{d\bar{P}}{dr}\right)^{-1}\right). \quad (2.42)$$

We now introduce a constant, ω_0, with units of angular velocity. This allows us to subtract $\omega_0\cdot$ (2.39) from (2.38); after using equation (2.42) for the term involving $u'P'$ the resulting equation is

$$\begin{aligned}\frac{\partial}{\partial t}\left[E' - \omega_0 M' + A\bar{h}^2 r(\bar{\omega}-\omega_0)\right] + \frac{\partial}{r\partial r}\left[\bar{h}r^2u'\left(\frac{gh'}{r} + v'(\bar{\omega}-\omega_0)\right)\right] &+ \\ \frac{\partial}{r\partial\phi}\left[A\bar{h}^2r^2\bar{\omega}(\bar{\omega}-\omega_0) + r(\bar{\omega}-\tfrac{1}{2}\omega_0)(gh'^2+\bar{h}v'^2)\right. &+ \\ \left. v'h'(g\bar{h} + r^2\bar{\omega}(\bar{\omega}-\omega_0)) + \tfrac{1}{2}r\bar{h}\omega_0 u'^2\right] &= 0 \quad (2.43)\end{aligned}$$

where $A = 1/2P'^2(d\bar{P}/dr)^{-1}$. Finally, integrating equation (2.43) over the domain we obtain

$$\frac{d}{dt}\iint\left[E' - \omega_0 M' + \bar{h}^2\left(\frac{d\bar{P}}{dr}\right)^{-1}\frac{1}{2}P'^2 r(\bar{\omega}-\omega_0)\right] r\,dr\,d\phi = 0. \quad (2.44)$$

We now argue that, if $E' - \omega_0 M' \geq 0$ and $(\bar{\omega} - \omega_0)d\bar{P}/dr \geq 0$, the constraint (2.44) does not allow P'^2 to grow in an overall sense. From (2.35) we note that $E' \geq 0$ if $\bar{v}^2 \leq g\bar{h}$. By a similar argument, $E' - \omega_0 M' \geq 0$ if $[r(\bar{\omega} - \omega_0)]^2 \leq g\bar{h}$. We can now state Ripa's shallow water generalization of the theorems of Rayleigh and Fjørtoft. *If there exists any value of* ω_0 *such that*

$$(\bar{\omega} - \omega_0)\frac{d\bar{P}}{dr} \geq 0 \qquad \text{and} \qquad [r(\bar{\omega} - \omega_0)]^2 \leq g\bar{h} \tag{2.45}$$

for all r*, then the flow is stable to infinitesimal perturbations.* Ripa has also discussed several corollaries of (2.45), one of which is obtained by choosing $\omega_0 = \max[\bar{\omega}]$. This results in the following weaker sufficient condition for stability. *If*

$$\frac{d\bar{P}}{dr} \leq 0 \qquad \text{and} \qquad \max[\bar{\omega}] \leq \min\left[\bar{\omega} + \frac{(g\bar{h})^{1/2}}{r}\right] \tag{2.46}$$

for all r*, then the flow is stable to infinitesimal perturbations.*

To recover the stability results for the nondivergent barotropic model from the stability results for the divergent barotropic model we consider the limit $g\bar{h} \to \infty$, in which case (2.45b) is satisfied for any finite ω_0. Then, there is no difference between vorticity and potential vorticity, and a choice of ω_0 such that $\bar{\omega}(r) < \omega_0$ everywhere leads to $d\bar{\zeta}/dr \leq 0$ everywhere as sufficient for stability, while a choice of ω_0 such that $\bar{\omega}(r) > \omega_0$ everywhere leads to $d\bar{\zeta}/dr \geq 0$ everywhere as sufficient for stability. Thus, a necessary condition for instability is that $d\bar{\zeta}/dr$ have both signs (Rayleigh's condition). It is also of interest to note that, if $d\bar{\zeta}/dr = 0$ at $r = \hat{r}$, then the choice $\omega_0 = \bar{\omega}(\hat{r})$ leads from (2.45a) to $[\bar{\omega}(\hat{r}) - \bar{\omega}(r)]d\bar{\zeta}/dr > 0$ somewhere in the flow as a necessary condition for instability (Fjørtoft's theorem).

2.3 Nonlinear stability - Arnol'd's theorem

In order to generalize the nondivergent linear arguments presented in section 2.1 to the nonlinear regime, we now begin with the nonlinear barotropic vorticity equation

$$\frac{D\zeta}{Dt} = \frac{\partial \zeta}{\partial t} + u\frac{\partial \zeta}{\partial r} + v\frac{\partial \zeta}{r\partial \phi} \quad = \quad 0, \tag{2.47}$$

where

$$\zeta \;=\; f + \frac{\partial(rv)}{r\partial r} - \frac{\partial u}{r\partial\phi} \tag{2.48}$$

is the absolute vorticity and the nondivergent wind components (u, v) satisfy the continuity equation

$$\frac{\partial(ru)}{r\partial r} + \frac{\partial v}{r\partial\phi} \;=\; 0. \tag{2.49}$$

We now divide the fields into basic state parts and parts associated with waves or eddies, e.g., $\zeta(r,\phi,t) = \bar{\zeta}(r) + \zeta'(r,\phi,t)$, where $\bar{(\;)}$ denotes the basic state part and $(\;)'$ the departure from the basic state. Here $\bar{(\;)}$ is not intended to refer to an integral function of the variable and $\bar{(\;)}' \equiv 0$ is not implied. In fact the basic state quantity for this case could also be a function of time although for the sake of simplicity we will consider it only a function of radius. No linearization will be performed so the primed variables do not necessarily have small amplitude. The ϕ-invariant basic state flow is assumed to be a steady solution of (2.47). We consider the case in which $\bar{\zeta}(r)$ is a monotonically decreasing function of r, and thereby define the inverse function $\bar{r}(\zeta)$ such that $\bar{r}(\bar{\zeta}(r)) = r$. Then, differentiating this last expression with respect to r, we obtain $\bar{r}_\zeta\bar{\zeta}_r = 1$. As the nonlinear generalization of the small amplitude wave-activity (2.29), we now follow McIntyre and Shepherd (1987), Shepherd (1988a) and Haynes (1988) to define the wave activity

$$A(\bar{\zeta},\zeta') \;=\; \int_0^{\zeta'} \tfrac{1}{2}\left[\bar{r}^2(\bar{\zeta}) - \bar{r}^2(\bar{\zeta}+\tilde{\zeta})\right] d\tilde{\zeta}. \tag{2.50}$$

If we approximate $\bar{r}(\bar{\zeta}+\tilde{\zeta})$ in (2.50) by the first two terms in a Taylor series expansion about $\bar{\zeta}$, it is easily shown that (2.50) reduces to (2.29). To derive the equation obeyed by $A(\bar{\zeta},\zeta')$ we first take the material derivative of this finite amplitude wave activity to obtain

$$\frac{DA}{Dt} \;=\; \frac{\partial A}{\partial\bar{\zeta}}\frac{D\bar{\zeta}}{Dt} + \frac{\partial A}{\partial\zeta'}\frac{D\zeta'}{Dt}, \tag{2.51}$$

where, from (2.50),

$$\frac{\partial A}{\partial\bar{\zeta}} \;=\; \tfrac{1}{2}r^2 - \tfrac{1}{2}\bar{r}^2(\bar{\zeta}+\zeta') + r\bar{r}_\zeta(\bar{\zeta})\zeta', \tag{2.52}$$

$$\frac{\partial A}{\partial\zeta'} \;=\; \tfrac{1}{2}r^2 - \tfrac{1}{2}\bar{r}^2(\bar{\zeta}+\zeta'). \tag{2.53}$$

Equations (2.52) and (2.53), together with the fact that $-D\zeta'/Dt = D\bar{\zeta}/Dt = u'\partial\bar{\zeta}/\partial r$, allow (2.51) to be written as

$$\frac{DA}{Dt} = ru'\zeta' = \frac{\partial\left[r^2u'v'\right]}{r\partial r} + \frac{\partial\left[\frac{1}{2}r(v'^2 - u'^2)\right]}{r\partial\phi}. \quad (2.54)$$

Using the nondivergence condition (2.49), equation (2.54) may be written in flux form

$$\frac{\partial A}{\partial t} + \frac{\partial\left[r(uA - ru'v')\right]}{r\partial r} + \frac{\partial\left[vA - \frac{1}{2}r(v'^2 - u'^2)\right]}{r\partial\phi} = 0. \quad (2.55)$$

Equation (2.55) is a finite-amplitude generalization of the linear wave activity relation (2.30). Several differences between equations (2.55) and (2.30) are noteworthy. The primed quantities in (2.30) are small amplitude, whereas the primed quantities in (2.55) may be of finite amplitude. Where the flux (uA, vA) appears in the finite amplitude relation (2.55), the flux $(0, \bar{v}A)$ appears in the small amplitude relation (2.30). Finally, the finite amplitude wave-activity is defined by (2.50), whereas the small amplitude wave-activity is defined by (2.29).

To obtain the nonlinear stability condition we now integrate (2.55) over the domain to obtain

$$\frac{d}{dt}\iint Ardrd\phi = 0. \quad (2.56)$$

Although this looks identical to (2.31), we must keep in mind that the A in (2.56) is defined by (2.50) while the A in (2.31) is defined by (2.29). The results are consistent since (2.50) reduces to (2.29) in the small amplitude limit. From the definition (2.50), we now note that

$$\frac{\frac{1}{2}\zeta'^2}{|\bar{\zeta}_r|_{\max}} = \int_0^{\zeta'} |\bar{r}_\zeta(\bar{\zeta})|_{\min}\tilde{\zeta}d\tilde{\zeta} \le |A(\bar{\zeta},\zeta')| \le \int_0^{\zeta'} |\bar{r}_\zeta(\bar{\zeta})|_{\max}\tilde{\zeta}d\tilde{\zeta} = \frac{\frac{1}{2}\zeta'^2}{|\bar{\zeta}_r|_{\min}}. \quad (2.57)$$

Together, (2.56) and (2.57) imply that

$$\begin{aligned}\frac{1}{|\bar{\zeta}_r|_{\max}}\iint \zeta'^2(r,\phi,t)rdrd\phi &\le \iint A(\bar{\zeta},\zeta',t)rdrd\phi \\ = \iint A(\bar{\zeta},\zeta',0)rdrd\phi &\le \frac{1}{|\bar{\zeta}_r|_{\min}}\iint \zeta'^2(r,\phi,0)d\lambda d\mu, \end{aligned} \quad (2.58)$$

which can also be written

$$\iint \zeta'^2(r,\phi,t)rdrd\phi \;\leq\; \frac{|\bar{\zeta}_r|_{\max}}{|\bar{\zeta}_r|_{\min}} \iint \zeta'^2(r,\phi,0)rdrd\phi. \tag{2.59}$$

This is the form of Arnol'd's (1965, 1966) result derived by McIntyre and Shepherd (1987) and used by Shepherd (1988a) to obtain rigorous bounds on the nonlinear saturation of barotropic instabilities to parallel shear flows. The inequality (2.59) bounds the disturbance enstrophy at time t in terms of the initial disturbance enstrophy and the radial gradient of the basic state absolute vorticity. It rules out the possibility of instability for basic state flows with $\bar{\zeta}_r > 0$ everywhere.

There are many interesting nonlinear aspects to the barotropic instability problem. Elegantly illustrated discussions of the nonlinear regime can be found in a paper by Lesieur et al. (1988) and in the recent textbook by Lesieur (1990, section 3.1 and Plates 7–8), who describe the time evolution of an unstable hyperbolic tangent shear layer in terms of the formation of fundamental eddies and the successive pairing or merging of these eddies.

Further insight into the nonlinear evolution of unstable waves in a vortex has been obtained by Dritschel (1986; 1989), using the method of contour dynamics (Zabusky et al. 1979, Zabusky and Overman 1983, Dritschel 1988). The method is specifically designed for piecewise-constant vorticity distributions such as the one used in our three region model. Basically, one simply predicts the position of the contours separating the regions of constant vorticity.

In concluding this section we would like to make two additional comments. First, by using the preceeding barotropic analysis we do not wish to imply that the dynamics of a vortex is a purely barotropic process. Certainly, baroclinic and moist physical processes must play an important role. However, there does appear to be a strong underlying component which is fundamentally barotropic in nature. Second, we note that the counterpropagating Rossby wave interpretation of barotropic instability is not the only way we can understand vortex instability. Another interpretation of barotropic instability is provided by an argument based on wave overreflection from critical radii (see Lindzen and Tung 1978, McIntyre and Weissman 1978, and the review article of Lindzen 1988).

According to this argument the Rayleigh and Fjørtoft necessary conditions for barotropic instability are also sufficient conditions for the existence of overreflected waves. The conditions are that $d\bar{\zeta}/dr$ change sign in the domain, that a critical radius exist, and that Rossby waves are overreflected at the critical radius and contained in such a way as to be repeatedly overreflected. Although considerable progress toward understanding barotropic and baroclinic instability can be made using the concepts of wave overreflection, the interpretation is more complex and perhaps less intuitive than the counterpropagating Rossby wave viewpoint.

Chapter 3

NORMAL MODE ANALYSIS

In this chapter we present the results of a normal mode analysis of the basic state conditions typical in the inner region of a tropical cyclone. The model is a nondivergent barotropic model. The basic state relative vorticity is represented in a piecewise constant manner with J steps, with the vorticity outside the radius r_J assumed to be that of the environment. The details of model development can be found in Appendix A. In the first section we will repeat the analysis of the three region version of this model first considered by Michalke and Timme (1967). In the second section we analyze the data compiled by Gray and Shea (1976) and several idealized profiles fit to that data. Finally, we offer an explanation for the formation of polygonal eyewalls based on further analysis of several idealized profiles.

3.1 Three region model

The distribution of relative vorticity for this model is shown in Figure 3.1. The eigensystem (A.21) reduces to

$$(\nu - \nu_1)\hat{\eta}_1 + \tfrac{1}{2}\xi_2(r_1/r_2)^{m-1}\hat{\eta}_2 = 0, \tag{3.1}$$

$$\tfrac{1}{2}\xi_1(r_1/r_2)^{m+1}\hat{\eta}_1 + (\nu - \nu_2)\hat{\eta}_2 = 0, \tag{3.2}$$

where $\nu_1 = m\hat{\omega}_1 - \frac{1}{2}\xi_1$ and $\nu_2 = m\hat{\omega}_2 - \frac{1}{2}\xi_2$ are the pure (noninteracting) Rossby wave frequencies at the inner and outer interfaces ,r_1 and r_2 respectively, and $\bar{\omega}_i = \bar{v}_i/r_i$ is the angular frequency at interface i. Thus the second term in equation (3.1) and the first term in equation (3.2) can be thought of as the measure of interaction between Rossby waves propagating at each interface. This equation shows that the degree of interaction will

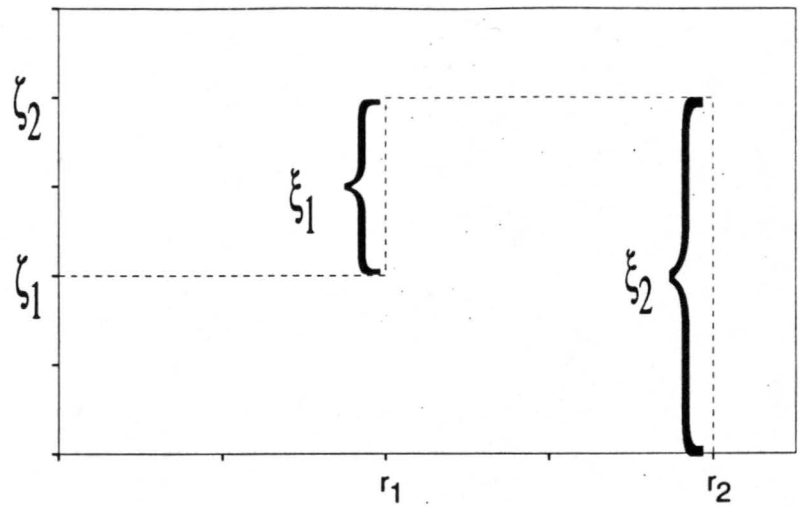

Figure 3.1: The basic state vorticity structure for the three region model.

decrease with increasing wavenumber or increasing distance between the interfaces (r_1/r_2 decreases). This is illustrated in Figure 3.2 in which we assume $\xi_1 = -\xi_2$ so that $\bar{\omega}_1 = 0$ and $\bar{\omega}_2 = \frac{1}{2}[(r_1/r_2)^2 - 1]$. Regarding (3.1) and (3.2) as a linear homogeneous system in the unknowns $\hat{\eta}_1$ and $\hat{\eta}_2$, we require that the determinant of the coefficient matrix vanish for nontrivial solutions, which yields the relation

$$\nu = \tfrac{1}{2}(\nu_1 + \nu_2) \pm \tfrac{1}{2}\left[(\nu_1 - \nu_2)^2 + \xi_1\xi_2(r_1/r_2)^{2m}\right]^{1/2}.$$

If we assume $\xi_1 = -\alpha\xi_2$ the condition for ν to be real is

$$\left[1 + \alpha\left(1 - m + mr^2\right)\right]^2 - 4\alpha r^{2m} \geq 0, \tag{3.3}$$

where $r = r_1/r_2$. When $\alpha = 1$ the system describes a cylinder of elevated vorticity surrounded by and surrounding areas of zero vorticity. Dritschel (1986) considered the nonlinear evolution of this system using a contour dynamics method. Several of his figures resemble the appearence of polygonal eyewalls, and allow us some insight as to the nonlinear extension of these results.

It can easily be shown that for $m = 0$ and $m = 1$, ν is real for all α, and for $m = 2$, ν is real for all $\alpha \leq 1$, and thus the vortex is stable, however for $m > 2$ instability may occur for values of $\alpha \leq 1$.

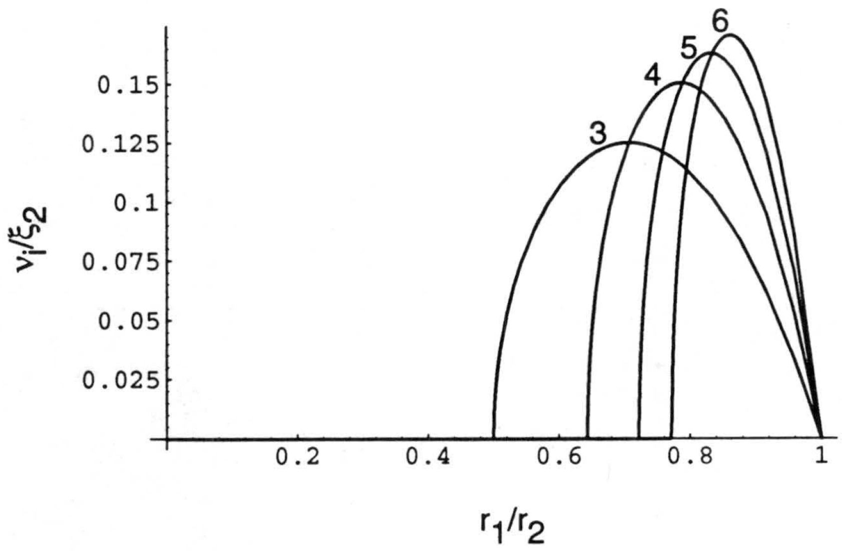

Figure 3.2: The normalized growth rate as a function of the width of a cylinder of elevated vorticity ($\xi_1 = -\xi_2$) for wavenumber 3, 4, 5, and 6 disturbances.

Michalke and Timme (1967) showed that the limiting case of an infinitely thin cylinder of elevated vorticity is always unstable for $m \geq 1$, and that for the case of a finite width instability may occur for all $m \geq 3$. They also showed that the presence of an elevated central vorticity does not always have the stabilizing effect one would expect. We illustrate this tendency with Figure 3.3 in which the maximum growth rate (normalized by the maximum vorticity) is contoured as a function of vorticity band width ratio, r_1/r_2 (x axis), and the angular velocity ratio, $\bar{\omega}_1/\bar{\omega}_2$ (y axis). Since $\bar{\omega}_1/\bar{\omega}_2 = (\xi_1 + \xi_2)/((r_1^2/r_2^2)\xi_1 + \xi_2)$, the y axis of Figure 3.2 is equivalent to the contours along the bottom ($\bar{\omega}_1 = 0$) edge of Figure 3.3. One might also notice the upper boundary of this figure ($\bar{\omega_1} = \bar{\omega}_2$) defines solid body rotation which is marginally stable to perturbations. For $r_1/r_2 < 0.5$ there is a region in which increasing the angular velocity in the inner region $r \leq r_1$ has the effect of producing an instability in wavenumber three where one did not exist before.

Eigensystems were calculated for wavenumbers 3 through 32. The transition from one wavenumber to the next occurs at the "V" in the contour. Unshaded areas are regions of stability except at the right edge of the graph where the greatest instabilities occur at higher wavenumbers than those computed here.

As a test of the usefulness of the semicircle theorem we also present Figure 3.4 which shows the normalized distance from the point $\omega_{max}/2$ to the point (ν_r, ν_i). Keeping in

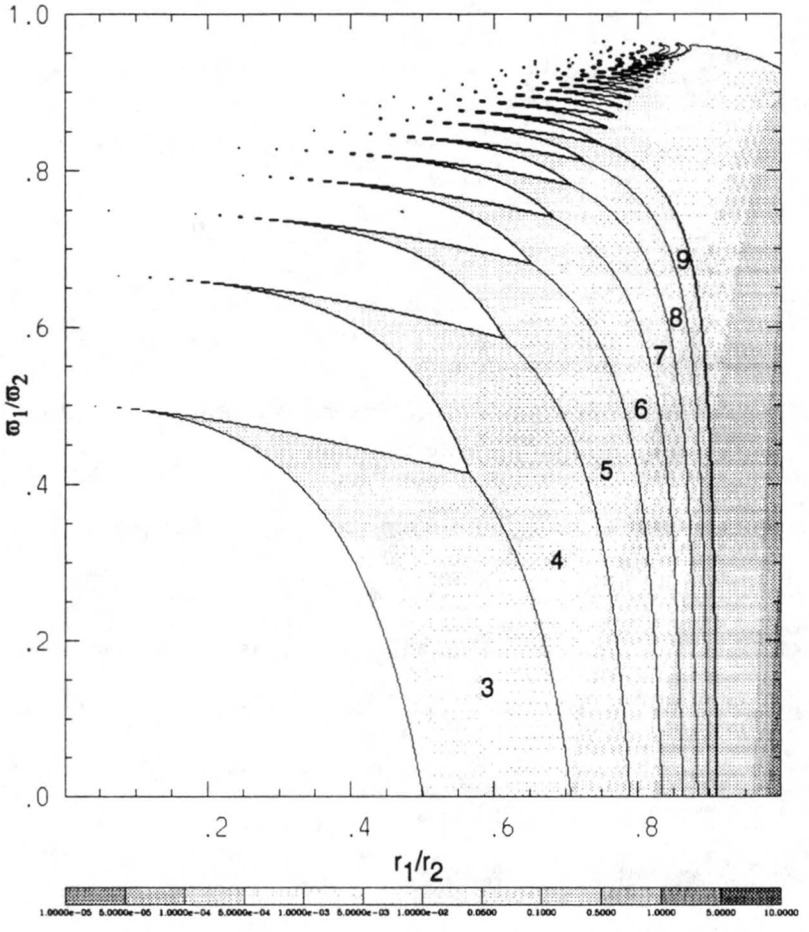

Figure 3.3: Wavenumber and growth rate of instabilities as a function of radius ratio and angular velocity ratio for the three region model. Wavenumbers 3 through 9 are indicated and calculations were made for all wavenumbers less than 16. Contours of growth rate increase logarithmically from lightest to darkest.

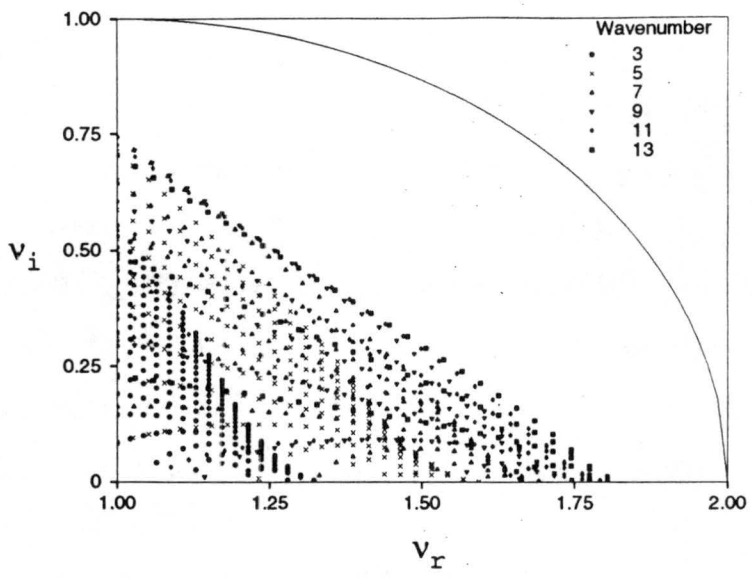

Figure 3.4: Scatter plot in the normalized (ν_r, ν_i) domain of unstable modes for the three region model with $\xi_1 = -\xi_2$ and varying r_1/r_2. The solid line is the limit described by equation (2.23). Only odd wavenumbers 3-13 are shown.

mind that these results are for the three region model only, we can observe from this figure that the upper bound described by the semicircle theorem becomes a better approximation as the wavenumber of the instability increases. This would suggest that there is a further dependence on wavenumber than that described by equation (2.23) on page 10. We should also note that, strictly speaking, the semicircle theorem as presented in section 2.1.2 is not valid for this problem since in 2.1.2 we implicitly assumed that the vorticity profile was smooth while here we allow discontinuities in that profile. It is also interesting to note that although the theory allows for growing instabilities at frequencies which are less than $\bar{\omega}_2$ (< 1 on the ν_r axis), none are found.

3.2 Analysis of hurricane inner core data

Gray and Shea (1976) presents an extensive set of data for hurricane flight penetrations between 1957 and 1969. There are approximately 100 aircraft flights into twenty-two hurricanes on forty-one storm days. The data is compiled into 2.5 nautical mile (nm) increments of radius from a minimum radius of 5 nm to a maximum radius of 50 nm. For each storm level between two and sixteen radial legs of data were collected, allowing us to approximate the radially averaged storm relative tangential wind..

A total of 492 radial legs are contained in the data set. From these we were able to compute 89 storm relative tangential wind profiles, each of which consists of averages at 19 radii. Table 3.1 gives the storm name, date, flight level, radius of maximum winds, and maximum tangential wind for each of the profiles analyzed. For details of the data collection and binning methods please refer to Shea (1972) and Gray and Shea (1976). Using equation (A.9) we can solve a linear system for the vorticity steps which exactly reproduce any discretely sampled profile of tangential winds. Since a realistic profile may have several reversals in gradient of vorticity we also present results for the best fit modified Rankine (e.g. Shea 1972) and Holland (1980) profiles, as well as two profiles which we shall call poly3 and poly4. A discussion of all of these profiles can be found in Appendix B. The best fit for each idealized profile was computed using the root mean square (RMS) error between the data and that profile. Using the 19 data points provided equation (A.9) was used to find the corresponding vorticity profile and the eigensystem (A.21) was then solved for the original data and each of the profiles using a double precision version of the real general matrix solver from the Eispack library. Since the velocity and not the vorticity was sampled, in the case of the idealized profiles, we should not expect the vorticity profile to reproduce exactly that given by the corresponding equations. Table 3.2 presents each profile from Table 3.1 by ID, the most unstable wavenumber and e-folding time for the data and each of the profiles, as well as the parameters used and the corresponding RMS error. The outer slope parameter for the poly3 and poly4 profiles is identical, thus only the poly3 value is shown.

At the bottom of the table a summary is provided which gives the number of unstable profiles, as well as the mean and standard deviation for each field.

Table 3.3 presents a summary by wavenumber of most unstable mode for the data and for each of the idealized profiles. Note that the data had at least one unstable mode in every case, while the idealized profiles often act in a stabilizing manner, reducing both the wavenumber and growth rate of the instability. The exception to this is the modified

Profile ID	Storm Name	Date	Approx. Flight Level (mb)	Radius of Maximum Wind (km)	Maximum Tangential Wind (m/s)
1	CARRIE	15-Sep-57	609	42	37
2	CARRIE	15-Sep-57	535	42	38
4	CARRIE	17-Sep-57	686	69	38
5	CARRIE	15-Sep-57	260	93	17
6	CLEO	18-Aug-58	811	42	35
7	CLEO	18-Aug-58	577	37	32
8	CLEO	18-Aug-58	260	88	17
9	DAISY	27-Aug-58	637	19	48
10	DAISY	27-Aug-58	270	19	32
11	DAISY	28-Aug-58	637	28	39
12	HELENE	25-Sep-58	811	46	32
14	HELENE	26-Sep-58	715	37	55
15	HELENE	25-Sep-58	577	32	49
16	HELENE	25-Sep-58	270	42	32
17	HANNAH	01-Oct-59	715	37	36
18	HANNAH	02-Oct-59	715	42	44
19	HANNAH	04-Oct-59	715	51	46
20	DONNA	04-Sep-60	618	23	60
22	DONNA	07-Sep-60	637	28	53
23	DONNA	09-Sep-60	811	28	61
24	ANNA	21-Jul-61	715	23	35
26	CARLA	08-Sep-61	715	60	40
27	CARLA	09-Sep-61	859	46	48
28	CARLA	09-Sep-61	859	32	49
29	CARLA	09-Sep-61	715	46	45
30	CARLA	10-Sep-61	618	37	46
31	CARLA	11-Sep-61	618	28	45
32	ESTHER	16-Sep-61	811	19	55
33	ESTHER	16-Sep-61	477	23	46
34	ESTHER	16-Sep-61	477	28	41
35	ESTHER	17-Sep-61	811	19	49
36	ESTHER	17-Sep-61	811	19	49
37	ESTHER	17-Sep-61	811	19	51
38	ELLA	10-Oct-62	907	56	39
39	ELLA	10-Oct-62	618	79	34
40	BEULAH	23-Aug-63	811	37	35
41	BEULAH	24-Aug-63	811	42	42
42	BEULAH	24-Aug-63	520	32	34
43	FLORA	03-Oct-63	715	19	53
44	FLORA	03-Oct-63	667	19	55
45	FLORA	10-Oct-63	715	79	35
46	FLORA	10-Oct-63	667	88	31
47	CLEO	23-Aug-64	715	14	57
48	CLEO	23-Aug-64	667	14	56
49	DORA	05-Sep-64	715	51	40
50	DORA	05-Sep-64	618	46	41
51	DORA	05-Sep-64	715	79	34
52	DORA	07-Sep-64	715	93	40
53	DORA	07-Sep-64	667	93	35
54	DORA	07-Sep-64	715	79	37
55	DORA	08-Sep-64	667	93	37
56	DORA	08-Sep-64	860	93	41
57	DORA	09-Sep-64	715	93	33
58	DORA	09-Sep-64	618	93	32
59	GLADYS	17-Sep-64	907	28	51
60	GLADYS	17-Sep-64	715	28	41
61	GLADYS	17-Sep-64	715	28	52
62	GLADYS	17-Sep-64	577	28	48
63	HILDA	01-Oct-64	907	23	48
64	HILDA	01-Oct-64	763	23	51
65	HILDA	01-Oct-64	667	28	42
66	HILDA	01-Oct-64	520	23	43
67	HILDA	01-Oct-64	322	23	48
68	HILDA	01-Oct-64	199	28	22
69	HILDA	02-Oct-64	907	46	44
70	HILDA	02-Oct-64	715	65	43
71	HILDA	02-Oct-64	667	74	42
72	HILDA	02-Oct-64	211	69	15
73	ISBELL	14-Oct-64	860	23	41
74	ISBELL	14-Oct-64	715	19	37
75	ISBELL	14-Oct-64	570	37	37
76	BETSY	03-Sep-65	763	46	46
77	BETSY	03-Sep-65	667	46	45
78	BETSY	03-Sep-65	520	32	41
79	BETSY	03-Sep-65	221	69	19
80	BETSY	05-Sep-65	907	69	50
81	BETSY	05-Sep-65	811	74	37
82	BETSY	05-Sep-65	667	69	33
83	BETSY	05-Sep-65	520	88	31
85	INEZ	27-Sep-66	763	14	38
86	INEZ	27-Sep-66	667	14	44
87	INEZ	27-Sep-66	520	14	32
88	INEZ	27-Sep-66	221	19	15
89	INEZ	28-Sep-66	955	14	60
90	INEZ	28-Sep-66	763	14	66
91	INEZ	28-Sep-66	667	14	55
92	INEZ	28-Sep-66	520	14	59
93	INEZ	28-Sep-66	221	19	27
94	BEULAH	18-Sep-67	955	42	35

Table 3.1: Storm profiles used in this study (from Gray and Shea (1976))

Profile ID	True MUW	e-folding time(hrs)	Rankine MUW	e-folding time(hrs)	Holland MUW	e-folding time(hrs)	Poly3 MUW	e-folding time(hrs)	Poly4 MUW	e-folding time(hrs)	Inner Rankine	Outer Rankine	Holland	Poly3 p	Poly3 z0	Poly4 z0	Rankine RMS Error	Holland RMS Error	Poly3 RMS Error	Poly4 RMS Error
1	3	2.27	11	40.43	2	2.32	2	6.92	2	5.03	1.28	-0.17	1.76	0.73	1.05e-09	9.85e-10	1.32	3.76	3.64	2.63
2	7	0.82	13	4.85	2	1.24	2	5.96	2	4.96	1.67	-0.24	2.01	0.92	7.00e-10	1.15e-09	1.65	4.41	4.80	3.63
4	7	1.17	*	*	2	2.05	2	18.62	2	11.87	1.24	-0.53	2.21	1.47	1.28e-10	1.38e-09	1.51	3.44	3.88	2.70
5	6	1.99	*	*	2	9.38	2	176.78	2	36.86	0.82	-1.97	1.42	0.10	1.00e-04	1.00e-04	0.81	2.43	1.87	1.83
6	5	2.91	*	*	2	1.51	2	6.40	2	5.68	1.21	-0.30	1.91	1.08	1.07e-10	3.07e-10	1.06	2.13	2.59	1.66
7	7	1.10	16	11.73	2	1.54	2	9.18	3	6.22	1.42	-0.19	1.66	0.76	1.77e-10	1.87e-10	1.00	3.69	3.10	2.51
8	6	2.85	*	*	2	6.39	2	55.53	2	44.63	0.96	-0.46	1.66	1.47	1.28e-10	1.86e-04	1.12	1.42	1.29	1.11
9	2	1.01	*	*	4	1.59	*	*	*	*	0.74	-0.58	1.90	1.22	4.27e-09	2.16e-03	1.07	2.49	3.03	2.91
10	2	3.33	5	1.07	3	0.99	*	*	4	1.96	2.21	-0.59	2.15	1.26	2.71e-09	1.78e-10	1.18	2.11	2.00	1.80
11	3	0.93	*	*	2	1.66	*	*	*	*	0.53	-0.36	1.40	1.02	3.19e-03	4.23e-03	1.25	1.56	0.66	0.79
12	4	2.99	*	*	2	1.69	3	40.59	2	7.08	1.08	-0.30	1.82	1.16	1.89e-10	2.61e-04	0.61	2.05	1.90	1.36
14	4	0.54	*	*	2	1.86	2	4.20	2	2.75	1.15	-0.47	1.99	1.31	1.20e-09	1.15e-10	5.00	4.72	6.15	4.95
15	4	1.12	15	7.44	2	0.79	2	3.66	2	2.35	1.42	-0.37	1.94	1.08	1.15e-09	1.45e-10	1.86	3.23	3.82	2.61
16	5	1.50	16	8.79	2	1.49	2	7.21	2	6.48	1.56	-0.33	2.19	1.14	1.89e-10	1.73e-10	0.91	2.70	2.99	2.15
17	10	1.67	13	6.10	2	1.35	3	11.62	3	6.39	1.53	-0.12	1.68	0.58	1.15e-09	1.66e-10	1.07	4.36	3.60	2.37
18	3	1.44	*	*	2	1.06	2	10.80	3	6.24	1.16	-0.48	2.03	1.41	1.18e-10	1.28e-10	2.08	1.86	3.09	1.61
19	4	3.22	16	47.77	2	1.32	2	7.77	4	11.39	1.30	-0.50	2.34	1.47	1.82e-10	2.22e-09	0.76	3.54	4.09	3.26
20	5	0.40	7	0.92	2	0.50	4	2.86	2	1.16	2.00	-0.65	2.33	1.40	2.71e-09	1.74e-09	2.22	3.73	5.10	4.27
22	5	0.69	9	1.71	2	0.72	2	2.69	3	2.15	1.79	-0.34	1.80	0.99	9.24e-10	1.49e-10	1.48	4.88	4.22	3.15
23	7	1.32	*	*	2	0.99	2	2.60	3	1.77	1.13	-0.56	2.04	1.34	2.61e-09	4.25e-05	0.88	3.18	3.77	3.10
24	9	2.55	*	*	3	1.56	6	10.13	4	5.42	0.67	-0.40	1.56	1.03	1.74e-09	2.59e-03	1.09	0.89	0.97	1.05
26	10	1.27	13	22.20	3	1.44	3	21.30	3	12.93	1.44	-0.32	2.52	1.47	6.84e-10	1.11e-09	1.35	4.26	4.35	3.50
27	7	1.38	14	48.43	2	1.20	3	15.79	2	4.21	1.29	-0.37	2.13	1.27	1.66e-10	1.01e-09	1.17	3.57	3.97	2.89
28	3	1.18	11	2.73	2	0.75	2	3.93	2	2.41	1.70	-0.38	2.05	1.12	1.10e-09	1.25e-10	1.75	3.51	4.59	3.32
29	3	2.17	*	*	2	1.31	3	16.48	2	5.77	1.12	-0.36	1.93	1.27	1.74e-09	2.89e-04	0.72	3.16	3.02	2.36
30	5	2.11	12	3.39	2	0.94	2	4.85	2	3.53	1.71	-0.41	2.23	1.22	1.27e-10	1.49e-10	0.86	4.10	4.83	3.66
31	4	1.79	*	*	2	1.08	2	3.18	3	2.74	1.21	-0.25	1.50	0.81	2.71e-09	1.28e-10	0.60	3.33	2.51	1.72
32	3	1.62	7	1.63	*	*	*	*	4	1.42	1.62	-0.27	1.28	0.74	6.79e-09	1.66e-10	2.36	6.22	5.55	4.98
33	2	1.19	10	4.07	3	1.10	6	15.87	2	1.88	1.50	-0.32	1.60	0.88	1.54e-09	1.16e-10	2.19	4.49	4.81	4.21
34	4	0.66	*	*	2	1.49	2	3.48	3	3.13	1.02	-0.22	1.42	0.72	1.07e-10	1.07e-08	3.81	4.44	4.70	4.25
35	2	2.73	*	*	*	*	*	*	4	1.75	0.90	-0.17	1.02	0.54	2.57e-09	2.99e-08	3.68	6.39	5.07	4.72
36	3	2.18	*	*	*	*	*	*	4	1.78	1.03	-0.16	1.02	0.54	5.08e-09	8.86e-10	2.27	5.53	3.73	3.37
37	2	1.05	*	*	*	*	*	*	4	1.67	1.17	-0.18	1.02	0.58	4.27e-09	1.15e-09	2.49	5.57	4.03	3.58

Table 3.2: Most unstable wavenumber (MUW) and e-folding time of instabilities for the Gray and Shea (1976) data and for profile fits as described in the text. Also included are best fit values and RMS error for each profile. (page 1 of 3)

Profile ID	True MUW	e-folding time(hrs)	Rankine MUW	e-folding time(hrs)	Holland MUW	e-folding time(hrs)	Poly3 MUW	e-folding time(hrs)	Poly4 MUW	e-folding time(hrs)	Inner Rankine	Outer Rankine	Holland	Poly3 p	Poly3 z0	Poly4 z0	Rankine RMS Error	Holland RMS Error	Poly3 RMS Error	Poly4 RMS Error
38	9	2.80	12	22.07	2	1.51	3	25.95	2	8.15	1.38	-0.19	2.26	1.02	1.07e-10	2.70e-09	1.09	4.39	4.22	3.27
39	11	1.14	8	110.25	2	2.28	2	53.85	2	13.81	1.31	-0.29	2.35	1.47	1.16e-10	1.15e-09	1.32	3.70	4.06	3.08
40	3	4.33	*	*	2	1.56	2	9.64	3	9.82	0.78	-0.15	1.34	0.68	1.74e-09	1.34e-03	1.30	1.90	1.23	1.05
41	2	2.73	*	*	2	2.26	2	5.26	2	6.53	1.07	-0.27	1.72	1.02	1.66e-10	3.32e-04	0.95	2.41	2.47	1.66
42	2	2.77	*	*	2	1.33	2	4.69	2	4.48	0.88	-0.30	1.48	0.95	1.82e-09	1.15e-03	0.82	2.34	1.94	1.80
43	3	0.73	*	*	*	*	*	*	4	1.31	1.10	-0.41	1.63	0.99	4.27e-09	1.15e-09	2.98	2.13	1.99	1.47
44	4	0.88	*	*	6	3.11	*	*	4	1.29	0.84	-0.51	1.79	1.12	6.43e-09	1.81e-04	1.47	2.43	2.76	2.50
45	7	2.99	*	*	2	4.15	3	77.58	4	153.35	0.70	-0.49	1.28	1.47	7.79e-04	1.08e-03	1.13	2.94	1.06	0.99
46	2	2.02	*	*	2	5.40	4	243.60	2	207.42	0.66	-0.69	1.26	1.47	7.87e-04	9.09e-04	1.25	3.12	1.34	1.18
47	2	4.00	*	*	*	*	*	*	*	*	0.66	-0.53	1.72	1.09	1.09e-08	6.79e-09	1.25	2.59	2.99	2.78
48	5	3.51	*	*	*	*	*	*	*	*	0.58	-0.52	1.70	1.07	1.75e-08	2.11e-03	1.07	3.13	3.51	3.45
49	10	1.49	*	*	2	2.11	*	*	*	*	0.40	-0.36	1.02	1.38	4.77e-03	3.62e-03	1.91	3.69	1.89	2.12
50	5	1.34	*	*	2	1.69	*	*	*	*	0.54	-0.38	1.12	1.30	3.22e-03	3.02e-03	0.58	3.95	1.77	1.90
51	2	3.46	*	*	2	4.97	*	*	*	*	0.27	-0.11	1.02	1.25	3.82e-03	2.74e-03	2.87	3.19	1.30	0.67
52	2	2.40	*	*	2	5.11	2	29.02	2	15.08	0.40	-1.97	1.02	0.10	1.00e-04	1.00e-04	2.28	4.55	6.07	9.19
53	4	2.98	*	*	2	5.89	2	31.28	2	17.45	0.30	-1.97	1.02	0.10	1.00e-04	1.00e-04	2.73	3.69	6.16	9.96
54	12	1.12	*	*	2	5.34	2	28.67	2	32.65	0.79	-0.15	1.41	1.46	3.54e-04	8.79e-04	1.31	3.25	1.55	1.73
55	4	3.08	*	*	2	4.39	2	30.08	2	16.25	0.74	-1.97	1.30	0.10	1.00e-04	1.00e-04	1.05	4.37	3.04	4.02
56	3	3.28	*	*	2	5.00	2	28.78	2	14.74	0.50	-1.97	1.02	0.10	1.00e-04	1.00e-04	1.30	3.88	3.70	7.04
57	10	3.78	*	*	2	6.20	2	32.44	2	18.57	0.42	-1.97	1.02	0.10	1.00e-04	1.00e-04	1.86	2.02	3.80	7.23
58	14	1.63	*	*	2	6.45	2	33.47	2	19.56	0.33	-1.97	1.02	0.10	1.00e-04	1.00e-04	2.13	3.15	5.34	8.43
59	2	1.08	*	*	2	0.71	2	2.86	3	2.21	1.06	-0.40	1.72	1.07	1.01e-10	2.96e-09	1.89	2.81	3.36	2.73
60	3	1.13	*	*	3	1.70	2	3.49	2	3.84	0.93	-0.21	1.35	0.72	1.43e-09	7.36e-04	1.55	3.44	2.56	2.14
61	3	0.47	*	*	2	1.42	2	2.89	3	2.07	1.21	-0.51	1.99	1.24	2.89e-09	1.15e-09	2.68	3.57	4.53	3.60
62	3	0.88	15	14.23	2	0.84	2	3.03	3	2.35	1.37	-0.40	1.82	1.06	1.49e-10	1.30e-10	1.68	3.41	4.05	3.09
63	7	1.54	*	*	4	1.60	6	11.22	2	1.80	1.03	-0.32	1.48	0.89	9.59e-10	6.81e-06	1.02	2.53	2.06	1.59
64	3	0.79	11	4.59	3	0.69	6	9.50	2	1.52	1.44	-0.44	1.80	1.08	3.29e-09	2.98e-09	1.20	3.88	4.63	3.80
65	3	1.66	*	*	2	0.99	2	3.95	2	6.44	0.70	-0.41	1.55	1.10	5.04e-04	2.98e-03	0.66	2.61	2.20	2.29
66	2	1.87	14	15.18	3	0.82	5	8.65	2	1.78	1.33	-0.45	1.80	1.10	4.40e-09	1.74e-09	0.79	2.48	3.18	2.53
67	4	1.25	8	1.55	2	0.58	5	4.70	2	1.52	1.84	-0.54	2.07	1.24	6.26e-09	1.74e-09	1.37	4.04	5.27	4.58
68	6	1.31	8	3.51	2	2.40	2	6.60	3	5.14	1.87	-0.38	1.88	1.05	1.15e-09	1.23e-09	1.64	2.74	2.53	2.38
69	4	1.99	*	*	2	2.03	2	11.96	2	12.21	0.79	-0.37	1.53	1.32	3.03e-04	1.67e-03	1.20	3.13	1.45	1.25
70	4	1.58	*	*	2	2.34	2	27.19	2	33.13	0.78	-0.33	1.34	1.47	9.26e-04	1.37e-03	1.25	4.91	2.80	2.66
71	11	0.93	2	8.21	2	4.87	*	*	*	*	0.59	-1.10	1.12	1.47	1.79e-03	1.80e-03	1.68	4.30	2.34	2.47
72	3	1.45	*	*	2	9.27	*	*	*	*	0.57	-0.40	1.02	1.47	8.22e-04	6.73e-04	1.28	2.50	1.76	1.83

Table 3.2: Most unstable wavenumber (MUW) and e-folding time of instabilities for the Gray and Shea (1976) data and for profile fits as described in the text. Also included are best fit values and RMS error for each profile. (page 2 of 3)

Profile ID	True MUW	e-folding time(hrs)	Rankine MUW	e-folding time(hrs)	Holland MUW	e-folding time(hrs)	Poly3 MUW	e-folding time(hrs)	Poly4 MUW	e-folding time(hrs)	Inner Rankine	Outer Rankine	Holland	Poly3 p	Poly3 z0	Poly4 z0	Rankine RMS Error	Holland RMS Error	Poly3 RMS Error	Poly4 RMS Error
73	6	0.66	*	*	2	1.14	*	*	*	*	0.49	-0.53	1.70	1.22	3.79e-03	5.20e-03	1.74	2.74	2.14	2.16
74	5	1.10	*	*	*	*	*	*	*	*	0.46	-0.29	1.23	0.79	1.24e-03	5.03e-03	1.52	0.85	0.55	0.68
75	2	0.48	*	*	5	8.06	*	*	*	*	0.22	-0.61	1.01	1.47	8.69e-03	5.61e-03	1.59	6.28	1.82	2.13
76	6	1.85	*	*	2	1.79	*	*	*	*	0.42	-0.37	1.04	1.30	5.09e-03	4.33e-03	1.82	3.02	1.29	1.35
77	2	1.33	*	*	2	1.73	*	*	*	*	0.43	-0.50	1.06	1.47	5.20e-03	4.23e-03	1.64	4.38	1.65	1.60
78	3	1.87	*	*	2	1.45	2	3.58	2	7.26	0.79	-0.20	1.31	0.77	3.23e-09	2.01e-03	0.93	2.27	1.26	1.23
79	5	2.29	*	*	2	6.48	*	*	*	*	0.56	-0.79	1.04	1.47	1.11e-03	1.02e-03	1.19	1.88	1.61	1.68
80	4	1.92	*	*	2	2.39	3	82.46	2	37.62	0.80	-0.55	1.23	1.47	1.24e-03	1.61e-03	3.11	7.44	5.26	5.22
81	9	1.45	*	*	2	3.67	*	*	*	*	0.44	-0.30	1.02	1.47	2.86e-03	2.29e-03	2.12	2.08	1.51	1.76
82	3	1.86	*	*	2	4.21	*	*	*	*	0.38	-0.30	1.02	1.47	3.30e-03	2.52e-03	2.34	2.14	1.56	1.49
83	2	3.41	*	*	2	8.14	*	*	*	*	0.32	-0.55	1.02	1.47	2.89e-03	1.99e-03	1.97	3.94	1.73	2.17
85	2	2.54	*	*	*	*	*	*	*	*	0.22	-0.38	1.38	0.88	1.00e-02	1.00e-02	0.67	0.74	0.93	1.05
86	5	1.12	5	1.50	*	*	*	*	*	*	1.75	-0.42	1.50	0.93	1.43e-08	8.18e-09	1.08	1.82	1.97	1.82
87	2	0.92	*	*	*	*	*	*	*	*	0.66	-0.26	1.08	0.70	5.78e-09	2.71e-09	1.60	1.39	1.25	1.19
88	4	0.71	*	*	*	*	*	*	*	*	0.70	-0.43	1.54	1.00	1.09e-04	1.69e-03	1.71	1.80	1.77	1.84
89	3	2.12	*	*	*	*	*	*	*	*	0.36	-0.51	1.67	1.06	1.84e-03	1.00e-02	2.13	0.73	1.00	1.13
90	2	1.82	*	*	*	*	*	*	*	*	0.71	-0.57	1.82	1.14	2.82e-08	6.79e-09	0.86	2.06	2.67	2.43
91	2	1.86	*	*	*	*	*	*	*	*	0.17	-0.50	1.63	1.05	1.00e-02	1.00e-02	1.58	0.98	1.28	1.49
92	4	2.28	*	*	*	*	*	*	*	*	1.01	-0.54	1.78	1.11	1.75e-08	6.79e-09	1.36	3.00	3.55	3.35
93	3	1.63	*	*	4	1.82	*	*	*	*	0.89	-0.60	1.95	1.28	5.89e-09	1.26e-03	1.94	1.24	1.05	1.19
94	3	1.91	*	*	2	2.02	*	*	*	*	0.50	-0.20	1.12	0.84	2.48e-03	2.90e-03	1.63	0.92	1.25	1.32
Count		89.00		25		73		54		61										
Mean		1.80		15.77		2.65		23.79		14.31	0.96	-0.52	1.57	1.05	9.19e-04	1.22e-03	1.58	3.17	2.92	2.75
Std dev		0.90		23.74		2.19		41.16		32.48	0.47	0.45	0.41	0.38	2.05e-03	2.15e-03	0.76	1.33	1.44	1.76

Table 3.2: Most unstable wavenumber (MUW) and e-folding time of instabilities for the Gray and Shea (1976) data and for profile fits as described in the text. Also included are best fit values and RMS error for each profile. A summary of mean and standard deviation of e-folding time is also shown. (page 3 of 3)

Rankine profile which often produces high wavenumber results, this is probably due to the discontinuity of basic state vorticity at the radius of maximum winds in this profile. The largest number of cases in the raw data occurred in wavenumbers two and three, while the mean most unstable mode was in wavenumber five. This agrees with the observations of Muramatsu (1986) who found square to hexagonal eyewalls to be most frequent. Nearly all of the cases were in wavenumbers (2-7). For the modified Rankine profile nearly all of the cases were stable, and of those which were unstable most occurred in higher wavenumbers. A comparison of these with the other three profiles in which all of the unstable modes were in wavenumber 6 or less indicates that spatially small anomalies in the tangential wind profile, such as the kink in the modified Rankine profile at the radius of maximum winds, tend to produce instabilities in higher wavenumbers while the smoothed profile (in which at most one reversal of vorticity occurs) tends to produce lower wavenumber instabilities, possibly at higher growth rates. Yet, the Rankine profile provided the best overall fit to the raw data in most individual profiles and in the average as indicated by the summary at the end of Table 3.2.

The largest growth rate, which occurred for profile #20, was in wave number five and corresponds to an e-folding time of about 24 minutes. The mean e-folding time for all profiles is about 1 hour 48 minutes. This time is well within the time scale of significance for tropical cyclones.

There does not seem to be a significant correlation between growth rate and most unstable wavenumber results for the raw data and any of the profiles. This would suggest that the most unstable mode is most dependent on the small scale structure of the velocity profile.

Figures 3.5 - 3.7 present the velocity and corresponding vorticity for several of the data profiles which were found to be most unstable. The corresponding idealized profiles are also shown for each case. For profile #75 the vorticity is maximum at the vortex center so that the instability is probably caused by the sharp decrease in velocity at 23 km just before increasing to the maximum. In fact it appears that in every case the instability is caused by sharp gradients in vorticity with small spatial extent. These anomalies may be

Wavenumber of MUM	Number of data Cases	Mean e-folding time(hrs)	Std Dev	Number of Rankine Cases	Mean e-folding time(hrs)	Std Dev	Inner parm	std dev	Outer parm	std dev	Number of Holland Cases	Mean e-folding time(hrs)	std dev	mean holland parm	std dev
2	20	1.56	2.35	1	4.87	*	0.59		-1.1		61	1.63	1.97	1.57	0.43
3	21	1.32	2.33	0	*	*					7	1.07	3.34	1.83	0.37
4	15	1.30	2.10	0	*	*					3	1.66	26.97	1.78	0.21
5	10	1.15	1.60	2	1.25	7.55	1.98	0.23	-0.5	0.09	1	8.05		1.01	
6	5	1.36	2.42	0	*	*					1	3.11		1.79	
7	7	1.29	4.03	2	1.18	4.27	1.81	0.19	-0.46	0.19	0				
8	0	*	*	3	3.20	3.84	1.67	0.26	-0.41	0.11	0				
9	3	2.09	6.66	1	1.71	*	1.79		-0.34		0				
10	4	1.73	5.13	1	4.07	*	1.5		-0.32		0				
11	2	1.03	10.44	3	4.93	7.16	1.47	0.17	-0.33	0.12	0				
12	1	1.12	*	2	5.87	8.01	1.55	0.16	-0.3	0.11	0				
13	0	*	*	3	7.23	14.70	1.55	0.1	-0.23	0.08	0				
14	1	1.62	*	2	23.15	44.23	1.31	0.02	-0.41	0.04	0				
15	0	*	*	2	9.78	31.18	1.4	0.02	-0.38	0.01	0				
16	0	*	*	3	13.62	25.72	1.43	0.11	-0.34	0.13	0				
Stable	0			64			0.73	0.3	-0.57	0.51	16			1.44	0.28

mean holland parm	std dev	Wavenumber of MUM	Number of Poly3 Cases	Mean e-folding time(hrs)	std dev	Mean p	std dev	Mean z0	std dev	Number of Poly4 Cases	Mean e-folding time(hrs)	std dev	Mean z0	std dev
1.57	0.43	2	38	6.12	8.47	0.93	0.46	7.33e-05	1.77e-04	38	4.53	4.71	3.97e-04	6.98e-04
1.83	0.37	3	8	23.15	40.79	1.21	0.28	2.53e-04	4.53e-04	13	3.31	6.24	1.07e-04	3.57e-04
1.78	0.21	4	2	5.66	5.79	1.44	0.03	3.94e-04	3.94e-04	10	2.10	3.74	3.86e-04	8.03e-04
1.01		5	2	6.09	20.58	1.17	0.07	5.33e-09	9.35e-10	0				
1.79		6	4	11.25	62.14	0.97	0.09	1.88e-09	8.62e-10	0				
		7	0							0				
		8	0							0				
		9	0							0				
		10	0							0				
		11	0							0				
		12	0							0				
		13	0							0				
		14	0							0				
		15	0							0				
		16	0							0				
1.44	0.28	Stable	35			1.12	0.28	2.18e-03	2.82e-03	28			3.16e-03	2.87e-03

Table 3.3: Summary of instabilities for data and related profiles by wavenumber

caused by errors in the data collection method. However, none of the anomalies are so questionable as to suggest that any of the data profiles are not physically realistic basic states.

3.3 Stability of an idealized profile

As we pointed out in the discussion of the three region model, counterpropagating waves will only interact with each other if they are sufficiently close together. In Figure 3.8 we have extended this interpretation to a somewhat more realistic vorticity profile by assuming a Gaussian distribution of vorticity with radius. We then sampled this vorticity at 64 points chosen with a constant vorticity step so that changes in growth rate and wavenumber should be due solely to the distance in radius between steps and not to the change in magnitude of the steps. The center of the profile is at sufficiently large radius that the vorticity is zero at small radius. As we would expect, if we consider the half-width of the Gaussian distribution to be a measure of the distance between waves, Figure 3.8 is quite similar to Figure 3.2. Note that wavenumber two is now included in the set of possibly unstable waves. The growth rate for this wave is generally much less than that for higher wavenumbers, however, it has an influence over a much greater distance. This factor certainly contributed to the findings of the previous section in which the three profiles which have a smooth gradient of vorticity throughout are most often unstable in wavenumber two when they are unstable at all, while the modified Rankine profile which has a discontinuity in the gradient of vorticity at the radius of maximum winds, most often produced high wavenumber instabilities. Another notable feature of this graph is that wavenumber 3 is never the most unstable wave. This may be significant for two reasons, first Muramatsu (1986) pointed out that he found no observations of triangular eyewalls, and second, Guinn (1992) could not produce a triangular feature in his nonlinear model unless his initial perturbation was also in wavenumber 3. On the other hand many of the data profiles analyzed in the previous section were most unstable in wavenumber 3.

Figures 3.9 and 3.10 show wavenumber 4 and 5 anomilies produced by using the modified Rankine profile out to the radius of maximum vorticity then decreasing the

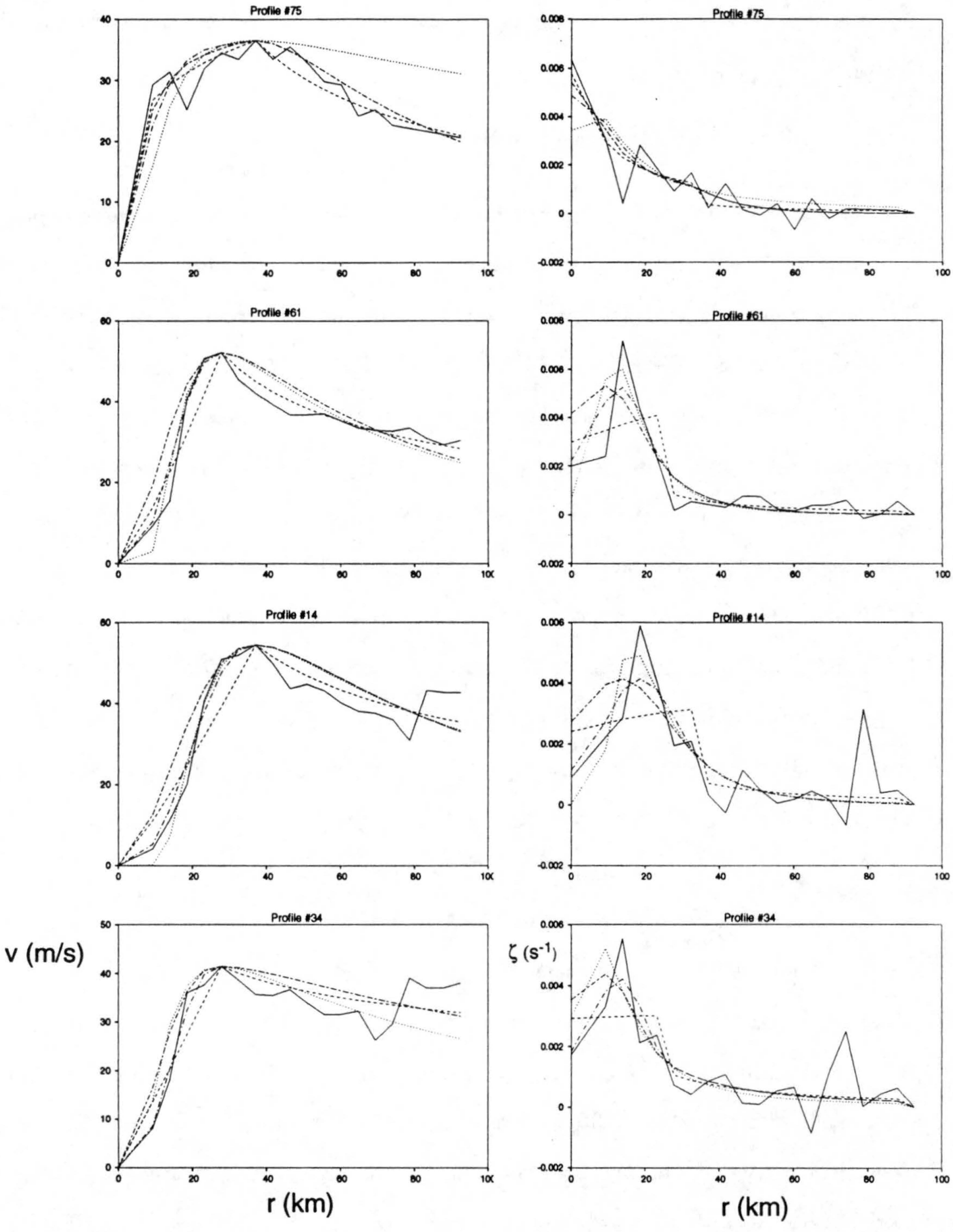

Figure 3.5: Profiles of mean tangential velocity (left figures) and the corresponding vorticity (right figures) for the data (solid), as well as the modified Rankine (dashed), Holland (dotted), Poly3 (chain dot), and Poly4 (chain dash) profile fits for selected storms. From top to bottom the corresponding most unstable wavenumbers for the raw data are (2,3,4,4).

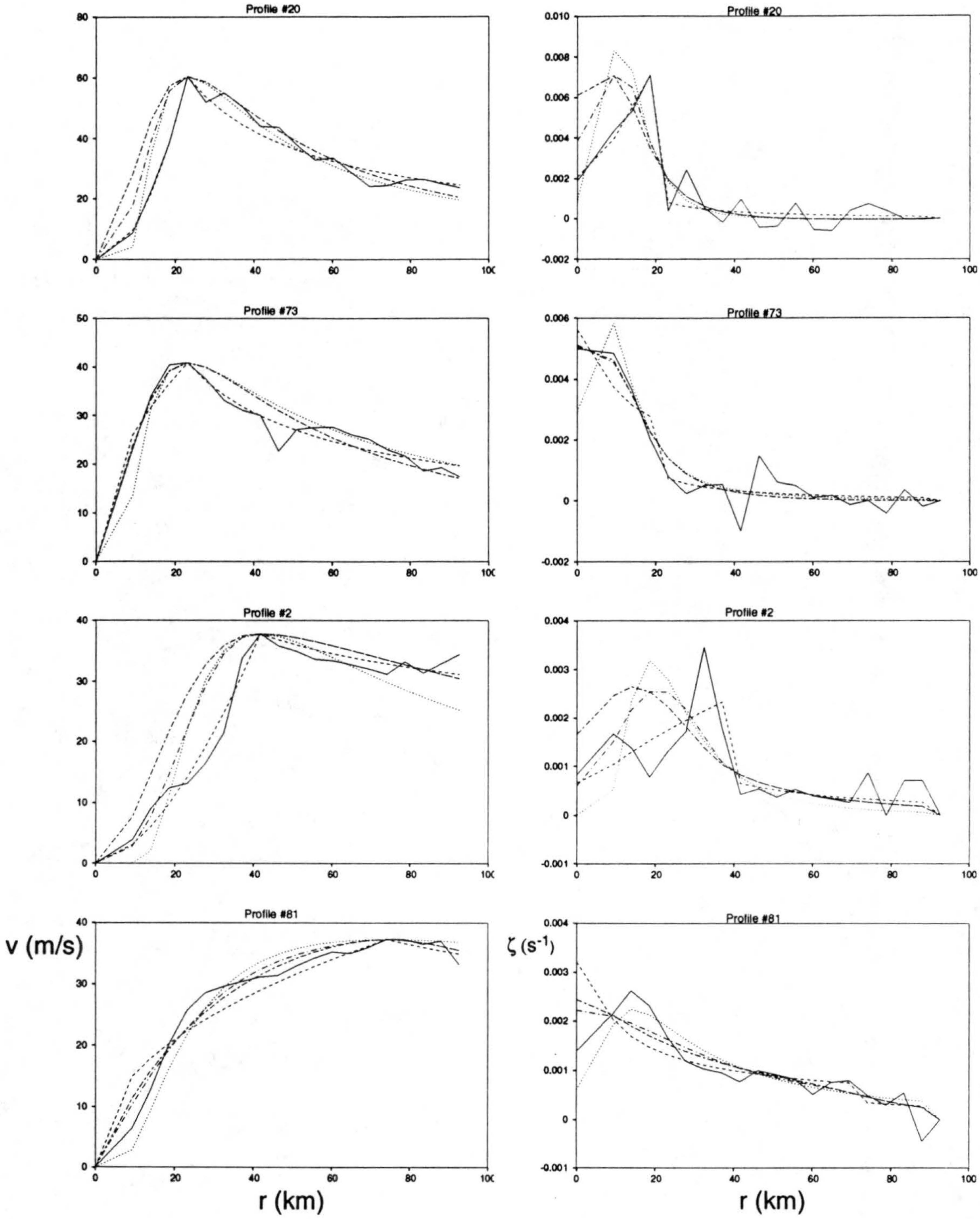

Figure 3.6: Same as Figure 3.5, except the most unstable wavenumbers are (5,6,7,9)

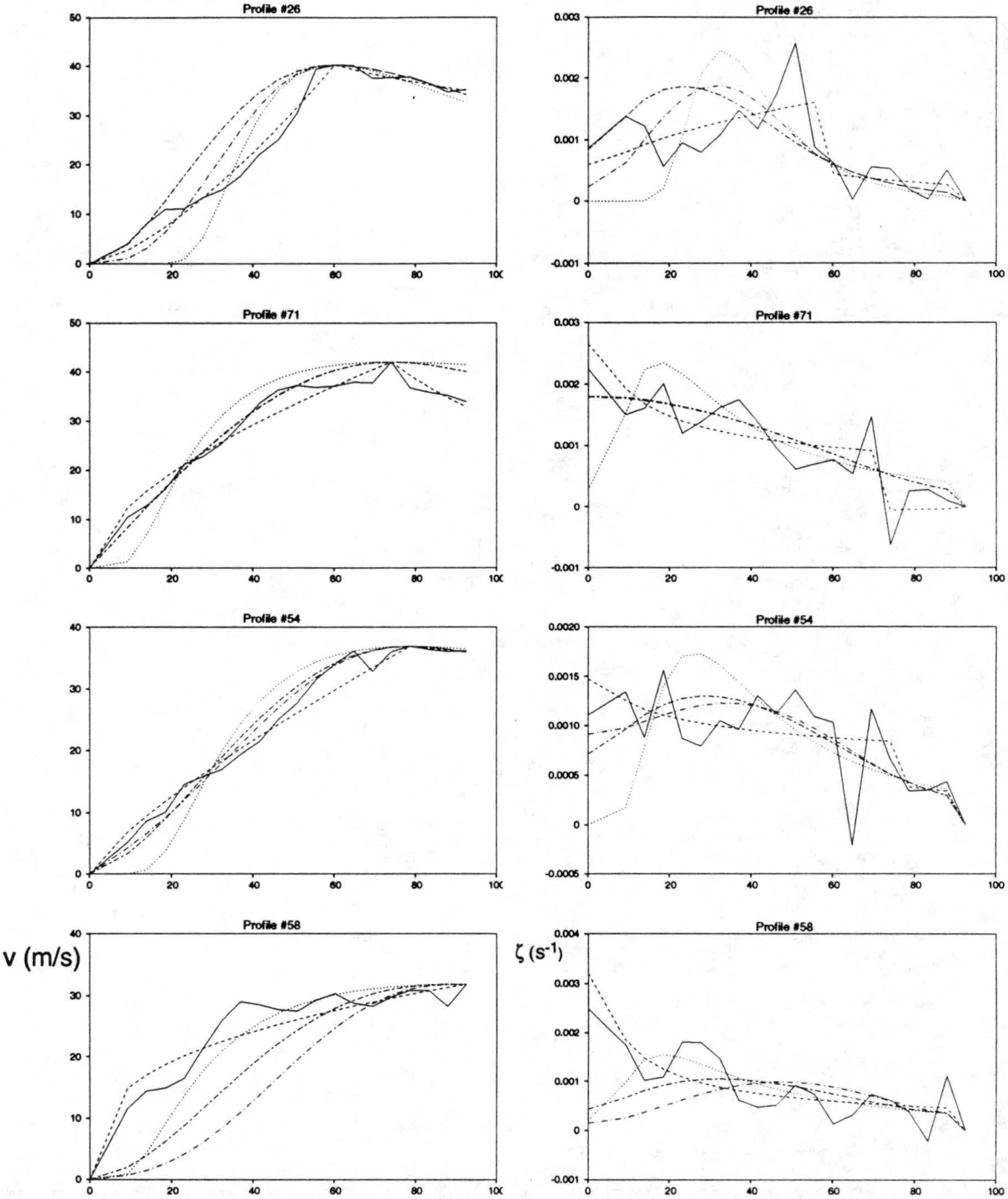

Figure 3.7: Same as Figure 3.5, except the most unstable wavenumbers are (10,11,12,14)

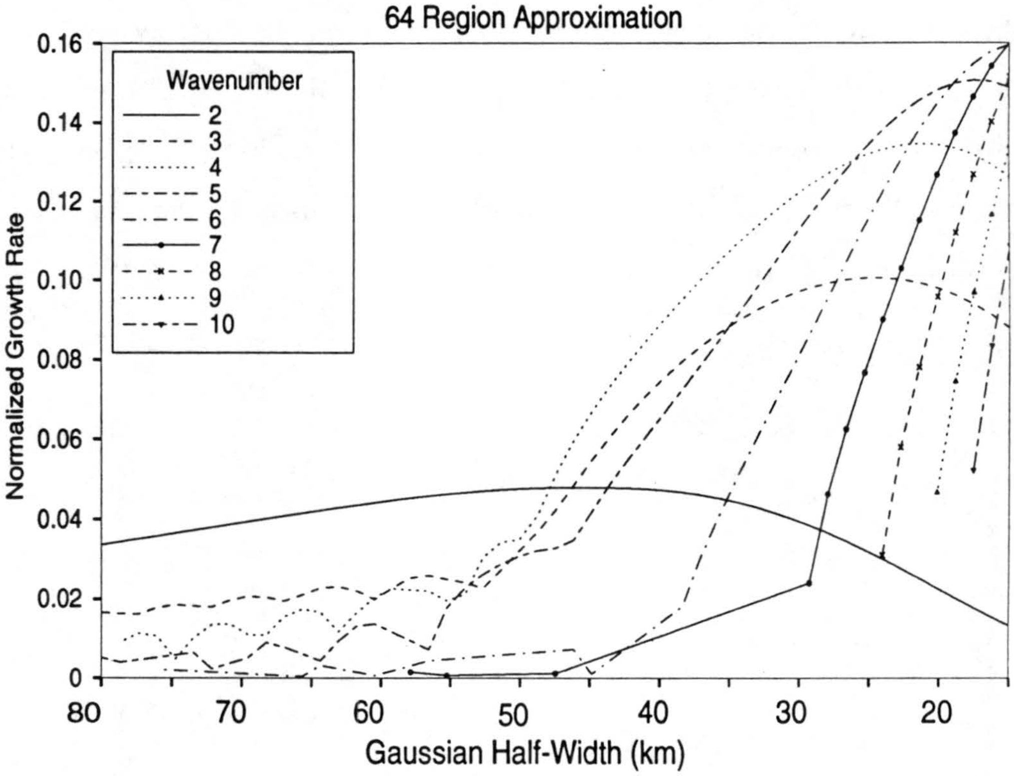

Figure 3.8: Growth rate of the most unstable mode in wavenumbers 2-10 for a Gaussian distribution of vorticity

vorticity linearly out to twice the radius of maximum vorticity. This is done to avoid the large change in vorticity of the modified Rankine profile at the radius of maximum wind. It also has the effect of shifting the radius of maximum wind to slightly greater radius with respect to the maximum vorticity. This test was also constructed so that the step size of vorticity remained constant rather than the sample radii. The upper figure is at some arbitrary time after an initial perturbation, the lower one is at one e-folding time later. The normalized basic state velocity and vorticity profiles are also shown, the difference between the basic states is best noticable in the vorticity profile which has a sharper gradient near the maximum for the wavenumber 5 case. Muramatsu (1986) observed several transitions of the eye of the same storm between wavenumbers four, five, and six. We have found that only slightly different basic states can produce maximum growth in any of these wavenumbers.

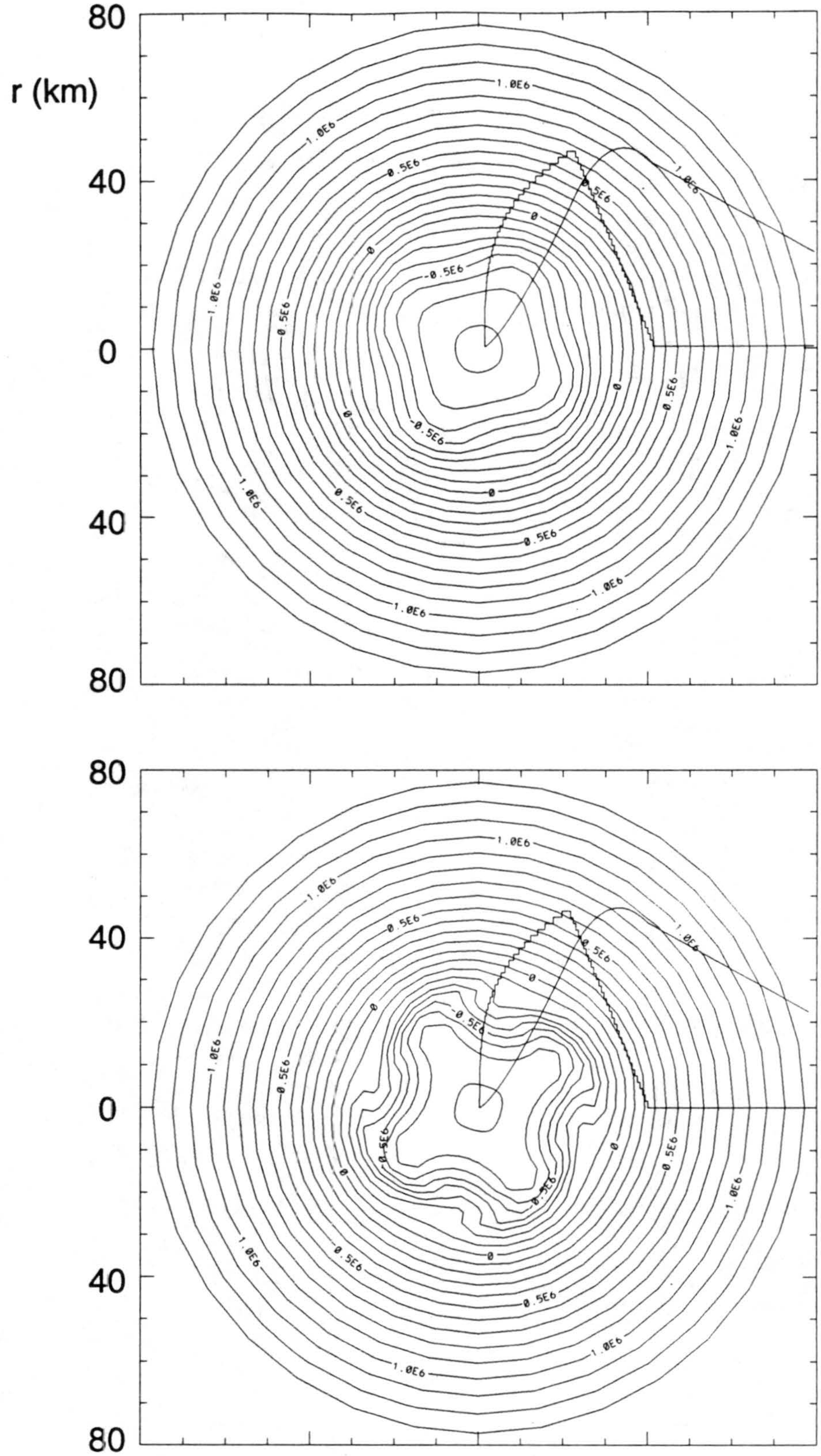

Figure 3.9: Wavenumber 4 streamfunction ($\bar{\psi} + \psi'$) field for a profile in which that is the most unstable mode. The normalized profiles of basic state velocity and vorticity are overlaid. The upper figure is at some arbitrary time, the lower one is one e-folding time later.

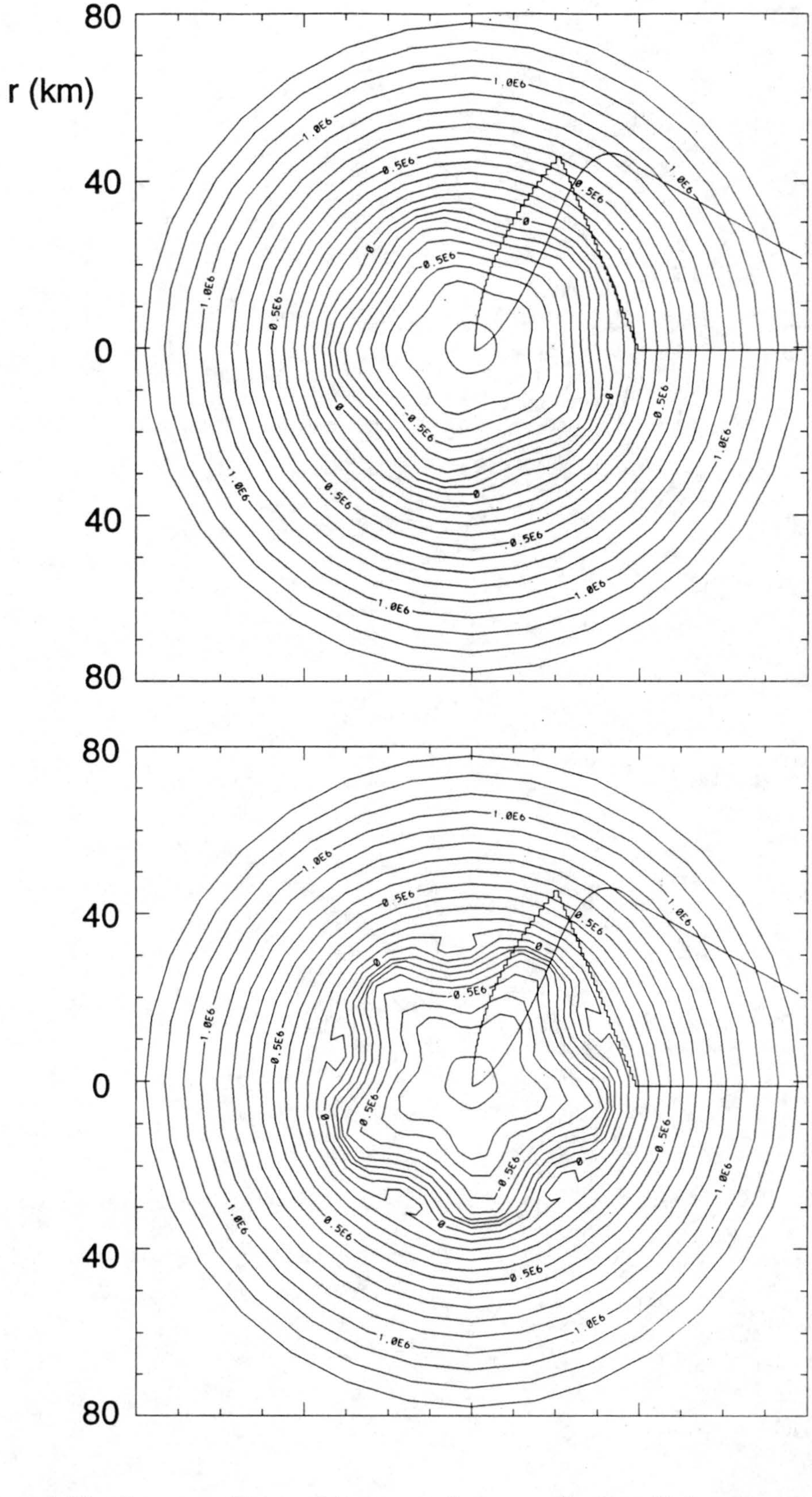

Figure 3.10: Same as Figure 3.9 except for a profile in which wavenumber 5 is most unstable.

Chapter 4

CONCLUSIONS

In this report we have reviewed the theory of barotropic stability of a hydrostatic inviscid shallow fluid on an f-plane. We have considered the divergent and non-divergent linear cases, (Rayleigh's, Fjørtoft's, and Ripa's theorems), and the non-linear, non-divergent case (Arnol'd's theorem). We believe this to be a reasonably complete summary of the theory of stability of a barotropic vortex as it is understood today.

We then developed a normal mode model, in which the axisymmetric basic state vorticity is approximated as a piecewise constant function, for the linear non-divergent case. Using this model we were able to analyze several profiles of storm relative tangential winds from the data set of Gray and Shea (1976). This analysis indicated that each of the profiles had instability in at least one mode and that these instabilities had e-folding times which were on the order of a few hours. These e-folding times appear to be short enough to influence the dynamics of a typical mature hurricane, although no attempt was made to verify their magnitude with another model. We then analyzed best fit profiles for each case using the modified Rankine, and Holland profiles as well as the poly3 and poly4 profiles developed in Appendix B. The results of this analysis indicate that smoother profiles have a stabilizing influence on the vortex. The modified Rankine profile was found to be the best overall fit with the smallest root mean square error and standard deviation over the entire dataset. However, it also typically gave instabilities in higher wavenumbers than the other profiles.

We have also shown observations (Figures 1.1 and 1.2) in which the eyewall structure is observed by radar or satellite to appear polygonal in shape and other observations of hurricanes which have indicated meso-vortices within the main storm, a phenomenon which is a logical non-linear extension of these polygonal features.

The polygonal perturbation produced in this model is often strongest near the radius of maximum winds. This polygonal feature can be extended to the vorticity field. However, there is little data available which details the vorticity in the inner region of a tropical cyclone. Therefore we can only intuitively assume that the fields of vorticity and those detectable by radar and satellite are somewhat correlated. Given this assumption it would appear that barotropic instability is the mechanism for these phenomena.

Clearly there is a need for more observational studies to either verify or refute the conclusions of this study. It seems worthwhile to repeat the eigenvalue calculations with a more accurate solver, such as that used in Weber and Smith (1994), and a model which assumes a smooth profile of vorticity instead of a piecewise constant profile as used here. It is also important to realize, as pointed out in Chapter 2, that the growth rates produced by normal mode analysis are not necessarily the largest growth rates possible for this type of instability. Instantaneous conditions forced by dynamics outside the realm of the linear nondivergent model may result in transient growth rates much larger than those produced by a normal mode model. The nonhomogeneous model developed in Appendix A can be used to investigate this possibility and perhaps to determine the optimal initial perturbation for wave growth.

It is also evident that a greater understanding can be had by extending this study to non-linear and three dimensional models. Work by Guinn (1992) and preliminary work by this author on a non-linear model would suggest that there may be a positive influence on wavenumber four perturbations due to the rectilinear nature of a cartesian coordinate model or to the rectilinear boundary conditions of that model, or perhaps both. On the other hand, Figure 3.8 indicates that we might expect wavenumber four to be dominant over a significant range of basic states. This would suggest the need for a study which compares the results of limited area nonlinear models in several coordinate systems.

REFERENCES

Andrews, D.G., 1983: A conservation law for small-amplitude, quasi-geostrophic disturbances on a zonally asymmetric basic flow. *J. Atmos. Sci.*, **40**, 85-90.

Arnol'd, V.I., 1965: Conditions for nonlinear stability of stationary plane curvilinear flows of an ideal fluid. *Dokl. Akad. Nauk.* SSSR, **162**, 975-978. (English translation: *Soviet Math.*, **6**, 773-777).

Arnol'd, V.I., 1966: On an a priori estimate in the theory of hydrodynamical instability. *Izv. Vyssh. Uchibn. Zaved. Mathematika*, **54**, no. 5, 3-5. (English translation: *American Math. Soc. Transl.*, Series 2, **79**, 267-269.

Black, P.G., and F.D. Marks, 1991: The structure of an eyewall meso-vortex in hurricane Hugo (1989). *Preprints from the 19th Conference on Hurricanes and Tropical Meteorology*, Amer. Met. Soc., 579-582.

Carr, L.E. III, and R.T. Williams, 1989: Barotropic vortex stability to perturbations from axisymmetry. *J. Atmos. Sci.*, **46**, 3177-3191.

Case, K.M., 1960: Stability of inviscid plane Coutte flow. *Physics of Fluids*, **3**, 143-148.

Charney, J.G. and M.E. Stern, 1962: On the stability of internal baroclinic jets in a rotating atmosphere. *J. Atmos. Sci.*, **19**, 159-172.

Drazin, P.G., and W.H. Reid, 1981: *Hydrodynamic Stability*, Cambridge University Press, New York. 525 p.

Dritschel, D.G., 1986: The nonlinear evolution of rotating configurations of uniform vorticity. *J. Fluid Mech.*, **172,** 157-182.

Dritschel, D.G., 1988: Contour Surgery: a topological reconnection scheme for extended integrations using contour dynamics. *J. Comput. Phys.*, **77**, 240-266.

Dritschel, D.G., 1989: On the stabilization of a two-dimensional vortex strip by adverse shear. *J. Fluid Mech.*, **206**, 193-221.

Eliassen, A., 1983: The Charney-Stern theorem on barotropic-baroclinic instability. *Pure Appl. Geophys.*, **121**, 563-572.

Emanuel, K.A., 1979: Inertial instability and mesoscale convective systems. Part I: Linear theory of inertial instability in rotating viscous fluids. *J. Atmos. Sci.*, **36** 2425-2449.

Farrell, B.F., 1987: Developing disturbances in shear. *J. Atmos. Sci.*, **44**, 2191-2199.

Flatau, M., and D.E. Stevens, 1989: Barotropic and inertial instabilities in the hurricane outflow layer. *Geophys. Astrophys. Fluid Dyn.*, **47**, 1-18.

Flatau, M., and D.E. Stevens, 1993: The role of outflow-layer instabilities in tropical cyclone motion. *J. Atmos. Sci.*, **50**, 1721-1733.

Fjørtoft, R., 1950: Application of integral theorems in deriving criteria of stability for laminar flows and for the baroclinic circular vortex. *Geofis. Publ.*, **17**, No 6, 52pp.

Franklin J.L., S.J. Lord, S.E. Feuer, and F.D. Marks Jr., 1993: The kinematic structure of hurricane Gloria (1985) determined from nested analysis of dropwindsonde and doppler radar data. *Mon. Wea. Rev.*, **121**, 2433-2451.

Gray, W.M., and D.J. Shea, 1976: Data summary of NOAA's hurricane flight penetrations 1957-1967, 1969. *Colorado State University*, Atmospheric Science Paper No. 257.

Guinn T.A. 1992: A dynamical theory for hurricane spiral bands. *Colorado State University*, Atmospheric Science Paper No. 497.

Haynes, P.H., 1988: Forced, dissipative generalizations of finite-amplitude wave-activity conservation relations for zonal and nonzonal basic flows. *J. Atmos. Sci.*, **45**, 2352-2362.

Holland, G.J., 1980: An analytic model of the wind and pressure profiles in hurricanes. *Mon. Wea. Rev.*, **108**, 1212-1218.

Lesieur, M., 1990: *Turbulance in Fluids.* Kluwer Academic Publishers, 412 pp.

Lesieur, M., C. Staquet, P. LeRoy, and P. Comte, 1988: The mixing layer and its coherence examined from the point of view of two-dimensional turbulence. *J. Fluid Mech.* **192**, 511-534.

Lewis, B.M., and H.F. Hawkins, 1982: Polygonal eye walls and rainbands in hurricanes. *Bull. Amer. Met. Soc.*, **63**, 1294-1300.

Lindzen, R.S., 1988: Instability of plane parallel shear flow (toward a mechanistic picture of how it works). *Pageoph*, **126**, 103-121.

Lindzen, R.S., and K.K. Tung, 1978: Wave overreflection and shear instability. *J. Atmos. Sci.*, **35**, 1626-1632.

Magnusdottir, G., and W.H. Schubert, 1990: On the generalization of semigeostrphic theory to the β-plane. *J. Atmos. Sci.*, **47**, 1714-1720.

Magnusdottir, G., and W.H. Schubert, 1991: Semigeostrophic theory on the hemisphere. *J. Atmos. Sci.*, **48**, 1449-1456.

McIntyre, M.E., and T.G. Shepherd, 1987: An exact local conservation theorem for finite-amplitude disturbances to non-parallel shear flows, with remarks on Hamiltonian structure and on Arnol'd's stability theorems. *J. Fluid Mech.*, **181**, 527-565.

McIntyre, M.E., and M.A. Weissman, 1978: On radiating instabilities and resonant over-reflection. *J. Atmos. Sci.*, **35**, 1190-1196.

Michalke, A. and A. Timme 1967: On the inviscid instability of certain two-dimensional vortex-type flows. *J. Fluid Mech.*, **29**, 647-666.

Möller, J.D., and R.K. Smith, 1994: The development of potential vorticity in a hurricane-like vortex. Submitted to *Q. J. R. Met. Soc.*

Muramatsu, T., 1986: The structure of polygonal eye of a typhoon. *J. Meteor. Soc. Japan*, **64**, 913-921.

Pedlosky, J., 1970: Quasi-geostrophic potential vorticity equation, *Geophysical Fluid Dynamics Summer School Notes*, Woods Hole Oceanographic Institution.

Ripa, P., 1983: General stability conditions for zonal flows in a one-layer model on the β-plane or the sphere. *J. Fluid Mech.* **126**, 463-489.

Ripa, P., 1991: General stability conditions for a multi-layer model. *J. Fluid Mech.*, **222**, 119-137.

Rotunno, R., 1986: Tornadoes and Tornadogenesis. *Mesoscale Meteorlogogy and Forecasting*, Edited by Ray, P. S., AMS, 414-436.

Schubert, W.H., and B.T. Alworth, 1987: Evolution of potential vorticity in tropical cyclones. *Q. J. R. Met. Soc.*, **113**, 147-162.

Shapiro, L.J., and M.T. Montgomery, 1993: A three-dimensional balance theory for rapidly rotating vortices. *J. Atmos. Sci.*, **50**, 3322-3335.

Shea, D.J., 1972: The structure and dynamics of the hurricane's inner core region. *Colorado State University*, Atmospheric Science Paper No. 182.

Shepherd, T.G., 1988a: Rigorous bounds on the nonlinear saturation of instabilities to parallel shear flows. *J. Fluid Mech.*, **196**, 291-322.

Shepherd, T.G., 1988b: Nonlinear saturation of baroclinic instability. Part I: The two-layer model. *J. Atmos. Sci.*, **45**, 2014-2025.

Shepherd, T.G., 1989: Nonlinear saturation of baroclinic instability. Part II: Continuously stratified fluid. *J. Atmos. Sci.*, **46**, 888-907.

Shepherd, T.G., 1990: Arnol'd stability applied to fluid flow: Successes and failures. *Proceedings of the IMA Workshop on Nonlinear Phenomena in Atmospheric and Oceanic Sciences*, June 4-8, 1990, G.F. Carnevale and R.T. Pierrehumbart, eds.

Smith, Gerald B. II, 1994: Studies of symmetrization in tropical cyclones. *MS Thesis*, Department of Atmospheric Science Colorado State University.

Snow, J.T., 1978: On inertial instability as related to the multiple-vortex phenomenon. *J. Atmos. Sci.*, **35**, 1660-1677.

Snow, J.T., 1982: A review of recent advances in tornado vortex dynamics. *Rev. Geophys. Space Phys.*, **20**, 953-964.

Staley, D.O., and R.L. Gall, 1979: Barotropic instability in a tornado vortex. *J. Atmos. Sci.*, **36,** 973-981.

Weber, H.C., and R.K. Smith, 1994: The stability of barotropic vortices: Implications for tropical cyclone motion Submitted to *Geophys. Astrophys. Fluid Dyn.*

Zabusky, N.J., M.H. Hughes, and K.V. Roberts, 1979: Contour dynamics for the Euler equations in two dimensions. *J. Comput. Phys.*, **30**, 96-106.

Zabusky, N.J., and E.A. Overman, 1983: Regularization of contour dynamical algorithms. *J. Comput. Phys.*, **52**, 351-373.

Appendix A

MODEL DEVELOPMENT

Here we derive the system used for normal mode analysis in Chapter 3 by two different methods. First we derive an eigen-equation for the nonlinear normal mode problem. This equation is then linearized into a standard eigenvalue problem which is solved for the complex frequency ν. Second we develop an initial value method which incorporates both the continuous spectrum and normal mode solution components using a Green's function approach starting from the linear system. This results in a nonhomogeneous system in which the algebraic spectrum is represented by the forcing term. This multiregion derivation is a natural extension of the two and three region formulation of Smith (1994).

A.1 Normal mode approach

We begin with the non-divergent shallow water model in cylindrical coordinates,

$$\frac{\partial u}{\partial t} - \zeta_a v + \frac{\partial}{\partial r}\left[gh + \tfrac{1}{2}(u^2+v^2)\right] = 0, \tag{A.1}$$

$$\frac{\partial v}{\partial t} + \zeta_a u + \frac{1}{r}\frac{\partial}{\partial \phi}\left[gh + \tfrac{1}{2}(u^2+v^2)\right] = 0, \tag{A.2}$$

$$\tfrac{1}{r}\frac{\partial r u}{\partial r} + \tfrac{1}{r}\frac{\partial v}{\partial \phi} = 0, \tag{A.3}$$

where u and v are the radial and tangential components of the horizontal wind, and $\zeta_a = f + \frac{\partial(rv)}{r\partial r} - \frac{\partial u}{r\partial \phi}$ is the absolute vorticity. This system has the properties that the relative vorticity, ζ, is conserved following a particle and that the components of flow can be described in terms of a single variable, the stream function, ψ, defined such that

$$u = -\frac{\partial \psi}{r\partial \phi} \quad \text{and} \quad v = \frac{\partial \psi}{\partial r}. \tag{A.4}$$

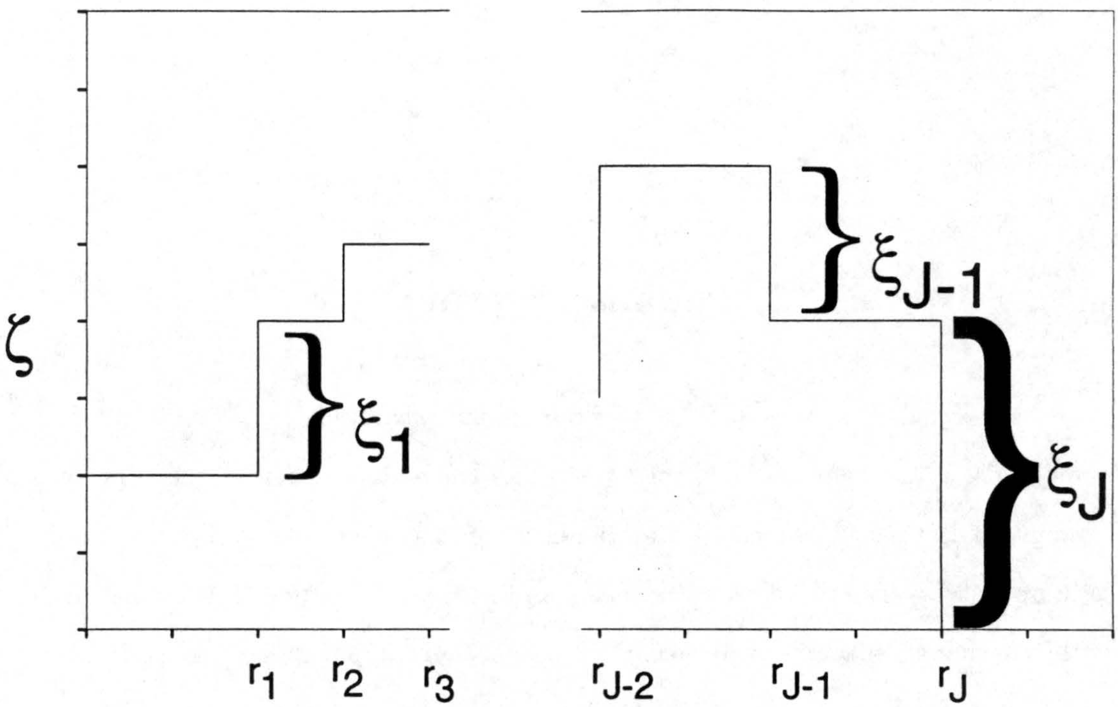

Figure A.1: An example of the basic state vorticity pattern assumed in this model.

We begin by defining an axisymmetric basic state relative vorticity field in a stepwise manner as

$$\bar{\zeta}(r) = \frac{\partial(r\bar{v})}{r\partial r} = \sum_{j'=j+1}^{J} \xi_{j'} \quad \text{for} \quad r_j < r < r_{j+1}. \tag{A.5}$$

where ξ_j is a (positive or negative) step of vorticity crossing $r = r_j$ inwards, and r_J is the radius beyond which the relative vorticity is identically zero. This profile is illustrated in Figure A.1 and can be thought of as a generalization of the two region case of a Rankine profile. Integrating this equation results in

$$r\bar{v}(r) = \int \left[r \sum_{j'=j+1}^{J} \xi_{j'} \right] dr \quad = \quad \frac{r^2}{2} \sum_{j'=j+1}^{J} \xi_{j'} + C_{j+1}. \tag{A.6}$$

We require that $r\bar{v}(r)$ is continuous at $r = r_j$ which gives

$$C_{j+1} \quad = \quad \frac{r_j^2}{2}\xi_j + C_j \tag{A.7}$$

Summing this recursive definition for C_j and applying the boundary condition $v(0) = 0$, (which requires C_1 0) we have

$$C_{j+1} = \sum_{j'=1}^{j} \frac{r_{j'}^2}{2} \xi_{j'}, \tag{A.8}$$

so that,

$$r\bar{v}(r) = \sum_{j'=1}^{j} \frac{r_{j'}^2}{2} \xi_{j'} + \sum_{j'=j+1}^{J} \frac{r^2}{2} \xi_{j'} \quad \text{for} \quad r_j \leq r \leq r_{j+1}. \tag{A.9}$$

We now integrate equation (A.9) to get the basic state streamfunction $\bar{\psi}(r)$ with the requirement that it remain bounded as r $0, \infty$ giving

$$\bar{\psi}(r) = \ln(r) \sum_{j'=1}^{j} \frac{r_{j'}^2}{2} \xi_{j'} + \frac{r^2}{4} \sum_{j'=j+1}^{J} \xi_{j'} C \quad {}_{1,j} + C_{2,j} \quad \text{for} \quad r_j \leq r \leq r_{j+1}. \tag{A.10}$$

To satisfy the boundary requirements we have $C_{1,1} = 0$ and $C_{2,J} = 0$, which gives, using recursive method outlined above,

$$C_{1,j} = -\sum_{j'=1}^{j} \ln(r_{j'}) \frac{r_{j'}^2}{2} \xi_{j'}, \tag{A.11}$$

$$C_{2,j} = -\sum_{j'=j+1}^{J} \frac{r_{j'}^2}{4} \xi_{j'}, \tag{A.12}$$

so that

$$\bar{\psi}(r) = \tfrac{1}{2} \sum_{j'=1}^{j} r_{j'}^2 \ln\left(\frac{r}{r_{j'}}\right) \xi_{j'} + \tfrac{1}{4} \sum_{j'=j+1}^{J} \xi_{j'} (r^2 \, r \quad {}_{j'}^{2}) \quad \text{for} \quad r_j \leq r \; r \quad {}_{j+1}. \tag{A.13}$$

We now define a perturbation streamfunction $\psi'(r, \phi, t) = \hat{\psi}(r) \exp[i(m\phi - \nu t)]$ with requirement that the perturbation vorticity $\zeta \quad '$ is identically zero everywhere except at the discontinuities of $\bar{\zeta}$, that is,

$$\frac{\partial}{r\partial r}\left(r \frac{\partial \hat{\psi}_j}{\partial r}\right) = \frac{m^2}{r^2} \hat{\psi}_j, \tag{A.14}$$

where $\hat{\psi} = \sum_{j'=1}^{J} \hat{\psi}_{j'}$. This equation is satisfied by

$$\hat{\psi}_j(r{=} \; C \quad {}_{1,j} r^{-m} \; C \quad {}_{2,j} r^m \quad \text{for} \quad r_j < r < r_{j+1}. \tag{A.15}$$

To insure that $\hat{\psi}(r)$ remains bounded throughout the domain we require that

$$\hat{\psi}_j = \begin{cases} C_{2,j} r^m & \text{for } r < r_j \\ C_{1,j} r^{-m} & \text{for } r > r_j \end{cases} .$$

Thus,

$$\hat{\psi}(r) = \sum_{j'=1}^{j} C_{1,j'} r^{-m} + \sum_{j'=j+1}^{J} C_{2,j'} r^m \quad \text{for} \quad r_j \le r \le r_{j+1}. \tag{A.16}$$

Requiring continuity of the radial wind at $r = r_j$ gives the relation $C_{1,j} = r_j^{2m} C_{2,j}$, which results in

$$\psi'(r,\phi,t) = \left[\sum_{j'=1}^{j} A_{j'} (r_{j'}/r)^m + \sum_{j'=j+1}^{J} A_{j'} (r/r_{j'})^m \right] e^{i(m\phi - \nu t)} \quad \text{for} \quad r_j \le r \le r_{j+1}, \tag{A.17}$$

where $A_j = C_{1,j} r_j^{-m} = C_{2,j} r_j^m$.

We now define the displacement of the j^{th} interface as $\eta_j(\phi, t) = \hat{\eta} \exp\left[i(m\phi - \nu t)\right]$ and require continuity of $rv = r\bar{v} + r\frac{\partial \psi'}{\partial r}$ at $r = r_j + \eta_j$ which results in

$$\tfrac{1}{2}\xi_j r^2 + A_j m \left(\frac{r}{r_j}\right)^m e^{i(m\phi - \nu t)} = \tfrac{1}{2}\xi_j r_j^2 - A_j m \left(\frac{r_j}{r}\right)^m e^{i(m\phi - \nu t)} \quad \text{at} \quad r = r_j + \eta_j. \tag{A.18}$$

Linearize this equation noting that $\eta_j \ll r_j$

$$m A_j \;=\; -\tfrac{1}{2}\xi_j r_j \hat{\eta}_j. \tag{A.19}$$

Now we observe that the radial velocity of a particle on an interface must be equal to that of the interface itself, i.e.,

$$\frac{\partial \eta_j}{\partial t} + \bar{v}_j \frac{\partial \eta_j}{r_j \partial \phi} \;=\; -\frac{im}{r_j} \psi'(r_j). \tag{A.20}$$

Combining (A.17), (A.19), and (A.20) we obtain a standard eigenvalue problem

$$(\nu - m\bar{v}_j/r_j)\hat{\eta}_j + \sum_{j'=1}^{J} \tfrac{1}{2}\xi_{j'} I_{jj'}^{(m)} \hat{\eta}_{j'} \;=\; 0, \tag{A.21}$$

where

$$I_{jj'}^{(m)} \;=\; \begin{cases} (r_{j'}/r_j)^{m+1} & \text{if } j' \le j \\ (r_j/r_{j'})^{m-1} & \text{if } j' \ge j \end{cases}$$

Equation (A.20) can be represented in matrix form as

$$\mathbf{A} = \begin{bmatrix} -m\bar{\omega}_1 + \frac{1}{2}\xi_1 & \frac{1}{2}\xi_2\left(\frac{r_1}{r_2}\right)^{m-1} & \frac{1}{2}\xi_3\left(\frac{r_1}{r_3}\right)^{m-1} & & \cdots & \frac{1}{2}\xi_J\left(\frac{r_1}{r_J}\right)^{m-1} \\ \frac{1}{2}\xi_1\left(\frac{r_1}{r_2}\right)^{m+1} & -m\bar{\omega}_2 + \frac{1}{2}\xi_2 & \frac{1}{2}\xi_3\left(\frac{r_2}{r_3}\right)^{m-1} & & \cdots & \vdots \\ \frac{1}{2}\xi_1\left(\frac{r_1}{r_3}\right)^{m+1} & \frac{1}{2}\xi_2\left(\frac{r_2}{r_3}\right)^{m+1} & \ddots & & \vdots & \vdots \\ \vdots & \vdots & \cdots & & \ddots & \frac{1}{2}\xi_J\left(\frac{r_{J-1}}{r_J}\right)^{m-1} \\ \frac{1}{2}\xi_1\left(\frac{r_1}{r_J}\right)^{m+1} & \cdots & \cdots & & \frac{1}{2}\xi_{J-1}\left(\frac{r_{J-1}}{r_J}\right)^{m+1} & -m\bar{\omega}_J + \frac{1}{2}\xi_J \end{bmatrix}.$$

A.2 Initial value problem

Consider the f-plane nondivergent barotropic vorticity equation linearized about a basic state $\bar{v}(r)$,

$$\frac{\partial \zeta'}{\partial t} + \bar{\omega}\frac{\partial \zeta'}{\partial \phi} + u'\frac{\partial \bar{\zeta}}{\partial r} = 0, \tag{A.22}$$

where $\bar{\omega} = \bar{v}/r$. Now define the basic state vorticity , $\bar{\zeta}$, in a piecewise constant manner as

$$\bar{\zeta} = \sum_{j'=j+1}^{J} \xi_{j}' \quad \text{for} \quad r_j < r < r_{j+1} \tag{A.23}$$

where ξ_j is a (positive or negative) step of vorticity crossing $r = r_j$ inwards, and the relative vorticity is identically zero outward from r_J. Integration of this equation results in

$$r\bar{v}(r) = \sum_{j'=1}^{j} \frac{r_{j'}^2}{2}\xi_{j'} + \sum_{j'=j+1}^{J} \frac{r^2}{2}\xi_{j'} \quad \text{for} \quad r_j \le r \le r_{j+1}. \tag{A.24}$$

With the definition (A.23) of $\bar{\zeta}$ equation (A.22) becomes

$$\frac{\partial \zeta'}{\partial t} + \bar{\omega}\frac{\partial \zeta'}{\partial \phi} = 0 \quad \text{for} \quad r \neq r_j. \tag{A.25}$$

We now perform a Fourier transform with respect to ϕ, defined as

$$f(k) = \int_0^{2\pi} f(\phi)\exp(im\phi)d\phi,$$

(It should be remembered that the Fourier space variables are different than their physical space counterparts although we choose not to change notation.)

$$\frac{\partial \zeta'}{\partial t} + \bar{\omega}im\zeta' = 0 \quad \text{for} \quad r \neq r_j \tag{A.26}$$

Define the streamfunction, ψ, such that $(u, v) = (-im\psi/r, \partial\psi/\partial r)$, with the usual relation to vorticity

$$\zeta = \nabla^2\psi = \left(\frac{\partial}{r\partial r}(r\frac{\partial}{\partial r}) - \frac{m^2}{r^2}\right)\psi. \tag{A.27}$$

Using equation (A.27) in equation (A.25) results in,

$$\left(\frac{\partial}{\partial t} + \bar{\omega} im\right)\left[\frac{\partial}{r\partial r}(r\frac{\partial}{\partial r}) - \frac{m^2}{r^2}\right]\psi' = 0 \quad \text{for} \quad r \neq r_j \tag{A.28}$$

We now further assume that ψ' can be written as a sum of functions,

$$\psi'(r,t) = \psi_a'(r,t) + \sum_{j=1}^{J} \lambda_j(t)\Psi j(r), \tag{A.29}$$

with the following properties:

- $\psi_a'(r,t)$ is analytic throughout the domain and at all times.
- Each $\Psi_j(r)$ is analytic throughtout the domain except at the point r_j where it is continuous.

We define a function to be analytic at a point if all of its derivatives exist at that point. A function is continuous at a point if it, but not nessasarily its deriviative, exists and is single valued at that point.

Equation (A.29) represents a linear combination of functions, thus each of the functions must also independently satisfy equation (A.28). In particular,

$$\left(\frac{\partial}{\partial t} + \bar{\omega} im\right)\left[\frac{\partial}{r\partial r}(r\frac{\partial}{\partial r}) - \frac{m^2}{r^2}\right]\psi_a' = 0, \tag{A.30}$$

throughout the domain since ψ_a' is analytic at all r_j. We can solve this using a Laplace transform defined as $f(s) = \int_0^\infty f(t)\exp(-st)dt$, thus

$$\left[\frac{d}{rdr}(r\frac{d}{dr}) - \frac{m^2}{r^2}\right][-\psi_{a0}' + s\psi_a'] + im\bar{\omega}\left[\frac{d}{rdr}(r\frac{d}{dr}) - \frac{m^2}{r^2}\right]\psi_a' = 0. \tag{A.31}$$

This can be rearranged into

$$\left[\frac{d}{rdr}(r\frac{d}{dr}) - \frac{m^2}{r^2}\right]\psi_a' = \frac{1}{s + im\bar{\omega}}\left[\frac{d}{rdr}(r\frac{d}{dr}) - \frac{m^2}{r^2}\right]\psi_{a0}', \tag{A.32}$$

and inverse transformed to

$$\left[\frac{d}{rdr}(r\frac{d}{dr}) - \frac{m^2}{r^2}\right]\psi'_a = \exp(-im\bar{\omega}t)\left[\frac{d}{rdr}(r\frac{d}{dr}) - \frac{m^2}{r^2}\right]\psi'_{a0}, \tag{A.33}$$

which can be expressed in terms of an initial vorticity perturbation, ζ_{s0} as

$$\left[\frac{d}{rdr}(r\frac{d}{dr}) - \frac{m^2}{r^2}\right]\psi'_a = \exp(-im\bar{\omega}t)\zeta_{s0}. \tag{A.34}$$

Equation (A.34), when multiplied by r is the cylindrical coordinate form of Euler's differential equation and can be solved using a Green's function approach. With the requirement that ψ_s be bounded for all r we arrive at

$$\psi'_a = \int_0^\infty G(r,\rho)\zeta'_{s0}(\rho)\exp(-im\bar{\omega}(\rho))\rho d\rho, \tag{A.35}$$

where

$$G(r,\rho) = \frac{-1}{2m}\begin{cases} \rho^{-m}r^m & \text{for } r \le \rho \\ \rho^m r^{-m} & \text{for } r \ge \rho \end{cases} \tag{A.36}$$

As a consequence of (A.29), $\nabla^2\Psi_j = \delta(r - r_j)$ where

$$\delta(x) = \begin{matrix} \infty & \text{for} & x = 0 \\ 0 & \text{for} & x \ne 0. \end{matrix} \tag{A.37}$$

Thus,

$$\left[\frac{d}{rdr}(r\frac{d}{dr}) - \frac{k^2}{r^2}\right]\Psi_j = \delta(r - r_j), \tag{A.38}$$

which is again a form of Euler's equation and has solution

$$\Psi_j = \frac{-1}{2m}\begin{cases} r_j^{-m+1}r^m & \text{for } r \le r_j \\ r_j^{m+1}r^{-m} & \text{for } r \ge r_j \end{cases} \tag{A.39}$$

We now require dynamic continuity at each interface r_j, that is, $h(r_j^+) = h(r_j^-)$ where $()^+$ is the limit when approached from greater values and $()^-$ is the limit when approached from below. From the tangential momentum equation

$$h = \frac{ir}{m}\frac{\partial v'}{\partial t} - r\bar{\omega}v' + \frac{ir}{m}\bar{\zeta}u', \tag{A.40}$$

which we can express in terms of the streamfunction as

$$h = \left(\frac{ir}{m}\frac{\partial}{\partial t} - r\bar{\omega}\right)\frac{\partial\psi'}{\partial r} + \bar{\zeta}\psi' \tag{A.41}$$

Thus,

$$h(r_j^+) - h(r_j^-) \quad = \quad \left(\frac{ir_j}{m}\frac{\partial}{\partial t} - r_j\bar{\omega}_j\right)\left(\left.\frac{\partial\psi'}{\partial r}\right|_{r_j^+} - \left.\frac{\partial\psi'}{\partial r}\right|_{r_j^-}\right) + \psi_j'\left(\bar{\zeta}(r_j^+) - \bar{\zeta}(r_j^-)\right) = 0, \quad \text{(A.42)}$$

From A.23 we have

$$\bar{\zeta}(r_j^+) - \bar{\zeta}(r_j^- \quad = \quad -\xi_j, \quad \text{(A.43)}$$

and integration of $r\cdot$ (A.38) from r_j^- to r_j^+ results in

$$\left(\left.\frac{\partial\Psi_j}{\partial r}\right|_{r_j^+} - \left.\frac{\partial\Psi_j}{\partial r}\right|_{r_j^-}\right) \quad = \quad 1. \quad \text{(A.44)}$$

Noting that all other terms of ψ' have the same limit at r_j when considered from either direction, we can use equations (A.43) and (A.44) in equation (A.42) to get,

$$\left(\frac{ir_j}{m}\frac{\partial}{\partial t} - r_j\bar{\omega}_j\right)\lambda_j - \xi_j\left(\psi_a' + \sum_{j'=1}^{J}\lambda_{j'}\Psi_{j'}\right) \quad = \quad 0. \quad \text{(A.45)}$$

Now use equation (A.39) and multiply by $-im/r_j$:

$$\frac{d\lambda_j}{dt} \quad = \quad i\left(-m\bar{\omega}_j\lambda_j + \tfrac{1}{2}\xi_j I_{jj'}^{(m)}\lambda_{j'} - \frac{m}{r_j}\xi_j\psi_a'(r_j)\right), \quad \text{(A.46)}$$

where

$$I_{jj'}^{(m)} \quad = \quad \begin{cases} (r_{j'}/r_j)^{m+1} & \text{if } j' \le j \\ (r_j/r_{j'})^{m-1} & \text{if } j' \ge j \end{cases}$$

Equation (A.46) represents a system of J ordinary coupled nonhomogeneous differential equations in λ and can be written in the form

$$\dot{\lambda} = i\mathbf{B}\lambda + i\mathbf{f}(t), \quad \text{(A.47)}$$

where

$$\mathbf{f}(t) \quad = \quad -\begin{bmatrix} \frac{\xi_1 m}{r_1}\psi_a'(r_1,t) \\ \vdots \\ \frac{\xi_J m}{r_J}\psi_a'(r_J,t) \end{bmatrix} \quad \text{(A.48)}$$

and

$$\mathbf{B} \quad = \quad \begin{bmatrix} -m\bar{\omega}_1 + \frac{1}{2}\xi_1 & \frac{1}{2}\xi_1\left(\frac{r_1}{r_2}\right)^{m-1} & \frac{1}{2}\xi_1\left(\frac{r_1}{r_3}\right)^{m-1} & \cdots & \frac{1}{2}\xi_1\left(\frac{r_1}{r_J}\right)^{m-1} \\ \frac{1}{2}\xi_2\left(\frac{r_1}{r_2}\right)^{m+1} & -m\bar{\omega}_2 + \frac{1}{2}\xi_2 & \frac{1}{2}\xi_2\left(\frac{r_2}{r_3}\right)^{m-1} & \cdots & \vdots \\ \frac{1}{2}\xi_3\left(\frac{r_1}{r_3}\right)^{m+1} & \frac{1}{2}\xi_3\left(\frac{r_2}{r_3}\right)^{m+1} & \ddots & \vdots & \vdots \\ \vdots & \vdots & \cdots & \ddots & \frac{1}{2}\xi_{J-1}\left(\frac{r_{J-1}}{r_J}\right)^{m-1} \\ \frac{1}{2}\xi_J\left(\frac{r_1}{r_J}\right)^{m+1} & \cdots & \cdots & \frac{1}{2}\xi_J\left(\frac{r_{J-1}}{r_J}\right)^{m+1} & -m\bar{\omega}_J + \frac{1}{2}\xi_J \end{bmatrix}.$$

The eigenvalues of the matrix $\mathbf{B}$ represent the solution for the homogeneous case ($\mathbf{f} \equiv \mathbf{0}$). If we compare this matrix to $\mathbf{A}$, we can see that

$$\mathbf{A} = \mathbf{D}^{-1}\mathbf{B}\mathbf{D}, \tag{A.49}$$

where

$$\mathbf{D} = \begin{bmatrix} \xi_1 & 0 & 0 & \cdots & 0 \\ 0 & \xi_2 & 0 & \cdots & \vdots \\ 0 & 0 & \ddots & 0 & \vdots \\ \vdots & \vdots & 0 & \ddots & 0 \\ 0 & \cdots & \cdots & 0 & \xi_J \end{bmatrix}. \tag{A.50}$$

Thus the matrices $\mathbf{A}$ and $\mathbf{B}$ are similar in the linear algebraic sense and as a consequence have identical eigenvalues.

Appendix B

TANGENTIAL WIND PROFILES

The modified Rankine profile is

$$v(r) \quad = \quad v_m \left(\frac{r}{r_m}\right)^p \tag{B.1}$$

where r_m = radius of maximum wind (RMW), $v_m = v(r_m)$ is the axisymmetric maximum tangential wind, and

$$p \quad = \quad \begin{array}{ll} p_i > 0 & \text{for } r \leq r_m \\ p_o < 0 & \text{for } r \geq r_m \end{array} \tag{B.2}$$

As shown in Chapter 3, this very simple profile often provides a very good fit to the observations. The mean relative vorticity associated with this profile is

$$\zeta(r) \quad = \quad (p+1)\frac{v_m}{r_m}\left(\frac{r}{r_m}\right)^{p-1} \tag{B.3}$$

Thus when $p_i = 1.0$ the inner vorticity is constant, otherwise the relative vorticity vanishes at storm center and increases out to the RMW where there is a discontinuity in the vorticity profile. Figure B.1 illustrates the structure of the modified Rankine profile for various values of p. Holland (1980) derived an axisymmetric tangential wind profile based on the pressure profiles of several Florida hurricanes. We can express this profile in terms of the radius and amplitude of maximum wind as

$$v(r) \quad = \quad v_m(\frac{r_m}{r})^{b/2} \exp\left(\tfrac{1}{2}(1-(\frac{r_m}{r})^b)\right). \tag{B.4}$$

with the realistic range for b as reported by Holland, $1 \leq b \leq 2.5$. The corresponding relative vorticity is

$$\zeta(r) \quad = \quad \frac{v_m}{2r_m}\left(\frac{r_m}{r}\right)^{b/2+1}\left(2-b+b\left(\frac{r_m}{r}\right)^b\right)\exp\left(\tfrac{1}{2}\left(1-\left(\frac{r_m}{r}\right)^b\right)\right). \tag{B.5}$$

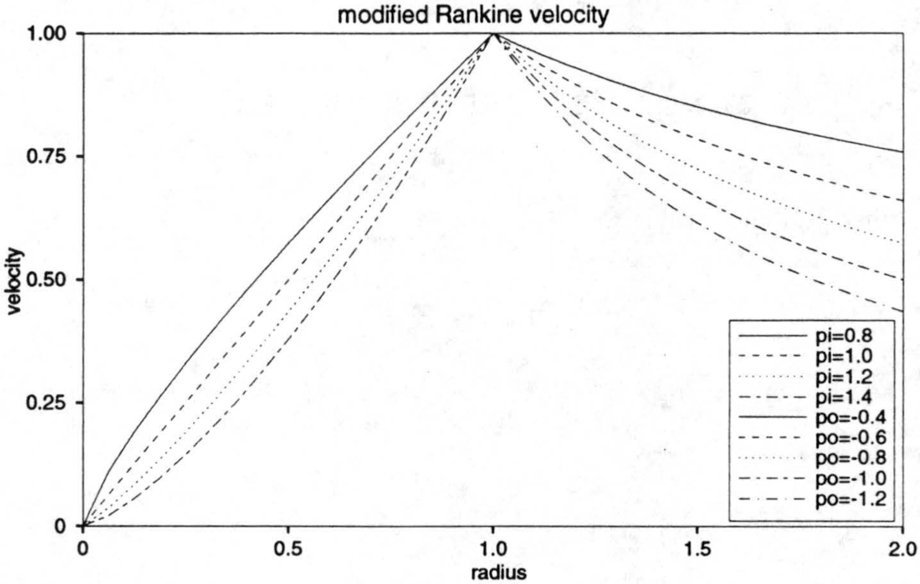

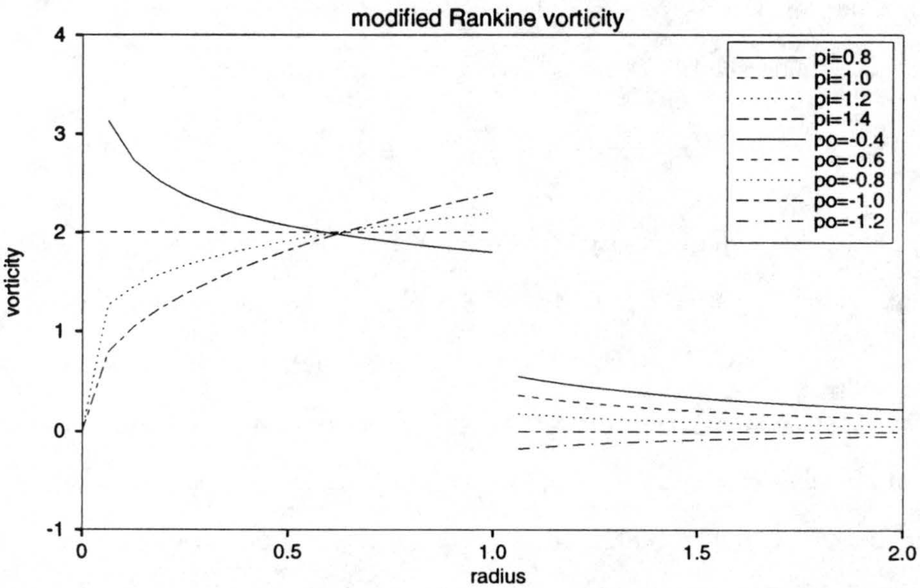

Figure B.1: Velocity (top) and vorticity structure of the modified Rankine profile. In this and the following figures all values are normalized to the RMW value.

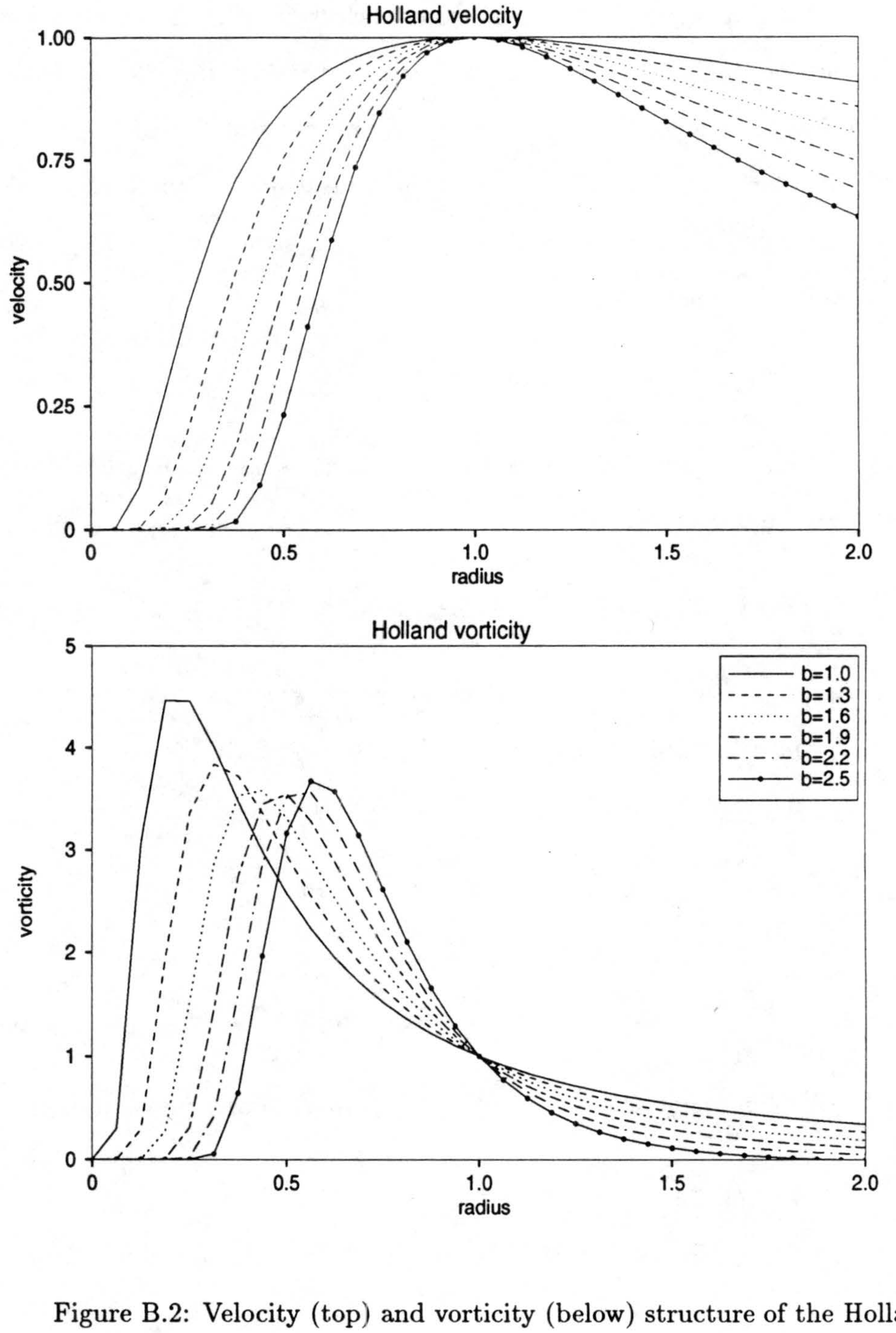

Figure B.2: Velocity (top) and vorticity (below) structure of the Holland profile.

For b in the range specified $\lim_{r\to 0}\zeta(r) = 0$ for this profile as shown in figure (B.2). We find it unlikely that the relative vorticity structure is constant within the RMW of a typical tropical cyclone, however it is also unlikely that the relative vorticity vanish completely at the storm center. We would like a manner in which to vary the inner core vorticity structure without varying that outside r_m, in order to consider the effects of different structures of inner core tangential winds on the barotropic stability of the vortex. A velocity profile in which the inner structure can be changed without modifying the outer structure is thus required. To do this we choose as an outer structure a slightly simplified version of the Holland profile above,

$$v(r) = v_m \left(\frac{r_m}{r}\right)^p \exp(1 - \left(\frac{r_m}{r}\right)^p) \quad \text{for} \quad r \geq r_m, \tag{B.6}$$

where v_m and r_m are as defined above, and p is a velocity slope parameter similar to b above. The corresponding vorticity is

$$\zeta(r) = \frac{v_m}{r} s^{-p} \left[1 + p(s^{-p} - 1)\right] \exp(1 - s^{-p}) \quad \text{for} \quad r \geq r_m, \tag{B.7}$$

where $s = r/r_m$. We now desire an inner region profile which is smoothly continuous at $r = r_m$, and which has $\zeta(0) = \zeta_0$. We do this in terms of a third order polynomial approximation to the vorticity profile,

$$\begin{aligned}\zeta(r) = \zeta_0 + \tfrac{3}{2}s&\left[\omega_{rmw}(12 - p^2) - 3\zeta_0\right] \\ +2s^2&\left[\omega_{rmw}(-16 + 2p^2) + 3\zeta_0\right] \\ +\tfrac{5}{2}s^3&\left[\omega_{rmw}(6 - p^2) - \zeta_0\right] \quad \text{for} \quad 0 \leq r \leq r_m,\end{aligned} \tag{B.8}$$

or, with the further constraint that $\frac{\partial\zeta}{\partial r} = 0$ at $r = 0$, a fourth order polynomial,

$$\begin{aligned}\zeta(r) = \zeta_0 + 2s^2&\left[\omega_{rmw}(20 - p^2) - 6\zeta_0\right] \\ +5s^3&\left[\omega_{rmw}(-15 + p^2) + 4\zeta_0\right] \\ +3s^4&\left[\omega_{rmw}(12 - p^2) - 3\zeta_0\right] \quad \text{for} \quad 0 \leq r \leq r_m,\end{aligned} \tag{B.9}$$

where $\omega_{rmw} = v_m/r_m$.

We can now compute the inner velocity based on each vorticity profile,

$$\begin{aligned} v(r) = r \Big\{ \frac{\zeta_0}{2} &+ s\left[\omega_{rmw}(6 - \tfrac{1}{2}p^2) - \tfrac{3}{2}\zeta_0\right] \\ &+ s^2\left[\omega_{rmw}(-8 + p^2) + \tfrac{3}{2}\zeta_0\right] \\ &+ s^3\left[\omega_{rmw}(3 - \tfrac{1}{2}p^2) - \tfrac{1}{2}\zeta_0\right]\Big\} \quad \text{for} \quad 0 \le r \le r_m \end{aligned} \tag{B.10}$$

and

$$\begin{aligned} v(r) = r \Big\{ \frac{\zeta_0}{2} &+ s^2\left[\omega_{rmw}(10 - \frac{p^2}{2}) - 3\zeta_0\right] \\ &+ s^3\left[\omega_{rmw}(-15 + p^2) + 4\zeta_0\right] \\ &+ s^4\left[\omega_{rmw}(6 - \frac{p^2}{2}) - \tfrac{3}{2}\zeta_0\right]\Big\} \quad \text{for} \quad 0 \le r \le r_m \end{aligned} \tag{B.11}$$

Figure (B.3) illustrates the structure of the poly3 and poly4 profiles and the effect of varying the $r = 0$ vorticity. Note that although the inner structure depends slightly on p the outer structure, illustrated by Figure B.4, is fully independent of ζ_0. The range of reasonable values for p is determined by the inertial stability, $I^2 = (f + \zeta_r)(f + 2v/r) > 0$, of the outer region. For equation (B.6), $v(r) > 0$ for all r so that this requirement reduces to $f + \zeta(r) \ge 0$. Differentiating equation (B.6) it follows that

$$\frac{\partial v}{\partial r} = \frac{v}{r}p(s^{-p} - 1) \quad \text{for} \quad r > r_m,$$

with this substitution we rewrite the inertial stability condition as

$$f + \frac{v}{r}\left[1 + p\left(s^{-p} - 1\right)\right] \ge 0$$

or,

$$s^{-p} \ge 1 - \frac{fr}{v} - \frac{1}{p}.$$

Clearly s^{-p} can become arbitrarily small as r gets large so that this equation can be true for all p only if $\frac{fr}{v} + \frac{1}{p} \ge 1$. The limiting case is now at $r = r_m$ so that $p \le \frac{R_m}{R_m - 1}$, where we have defined the Rossby number for the storm as $R_m = v_m/(fr_m)$.

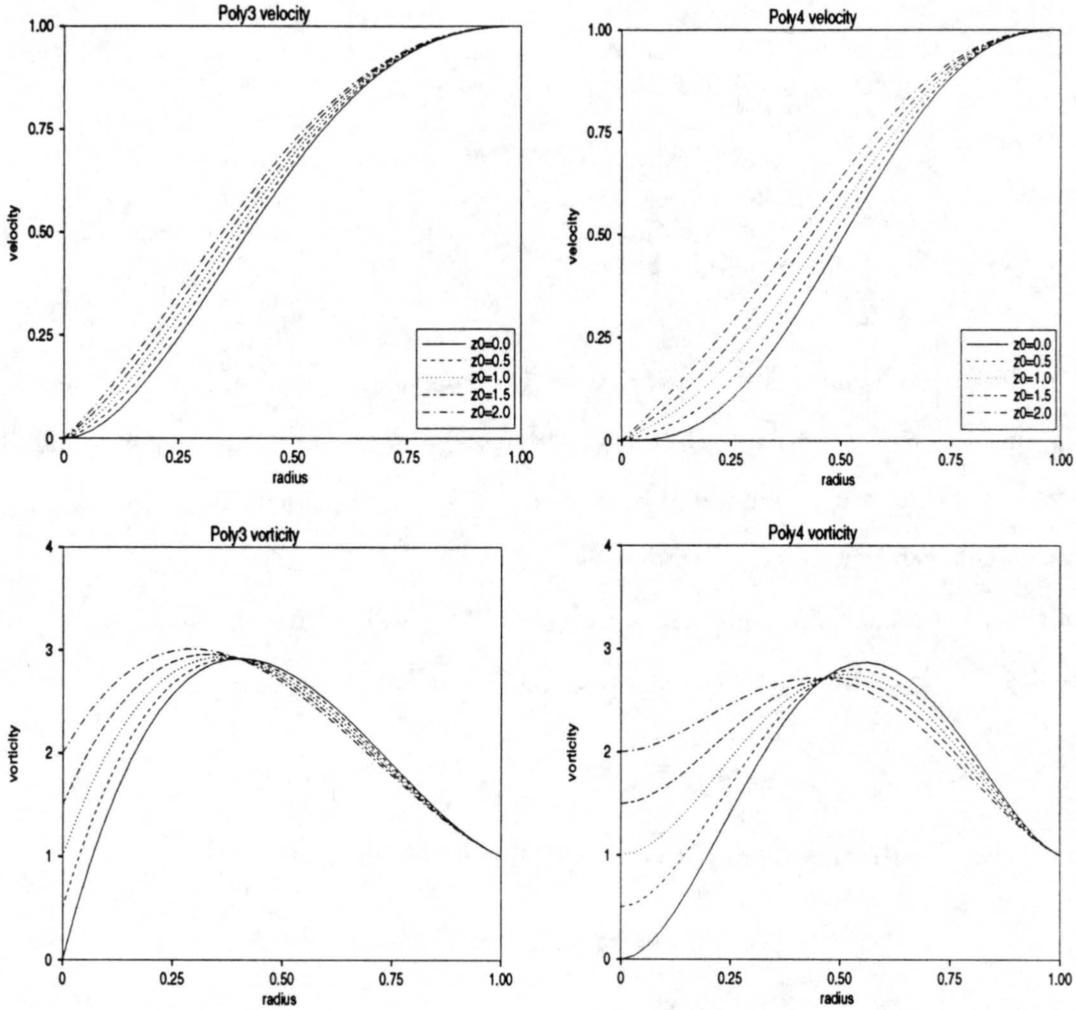

Figure B.3: Velocity (top) and vorticity (below) structure of the poly3 (left) and poly4 (right) profiles out to RMW. Here $z0 = \zeta_0$, and $p = 1.0$.

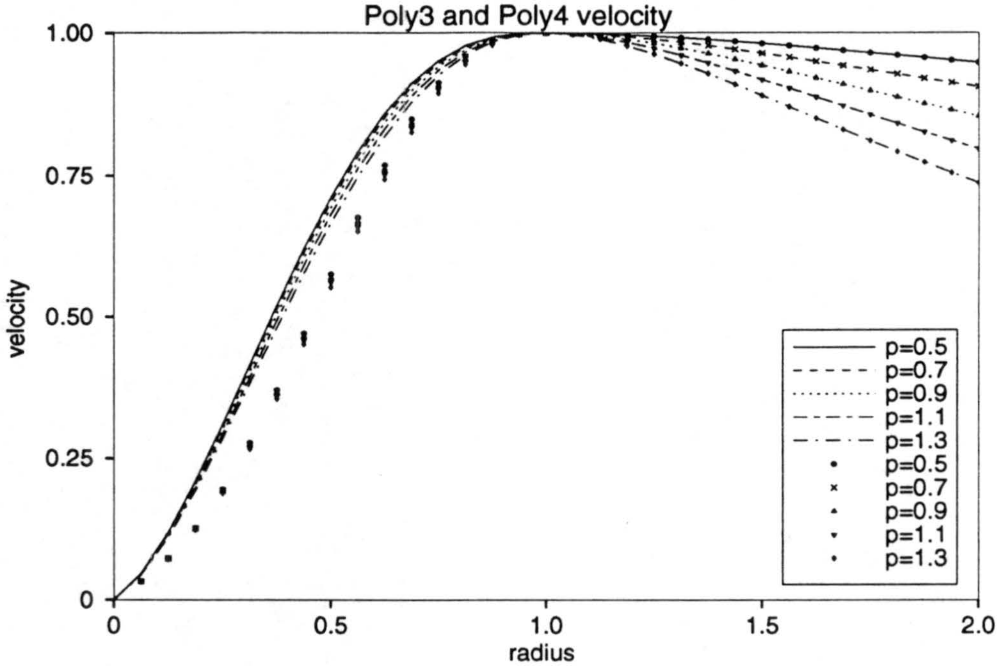

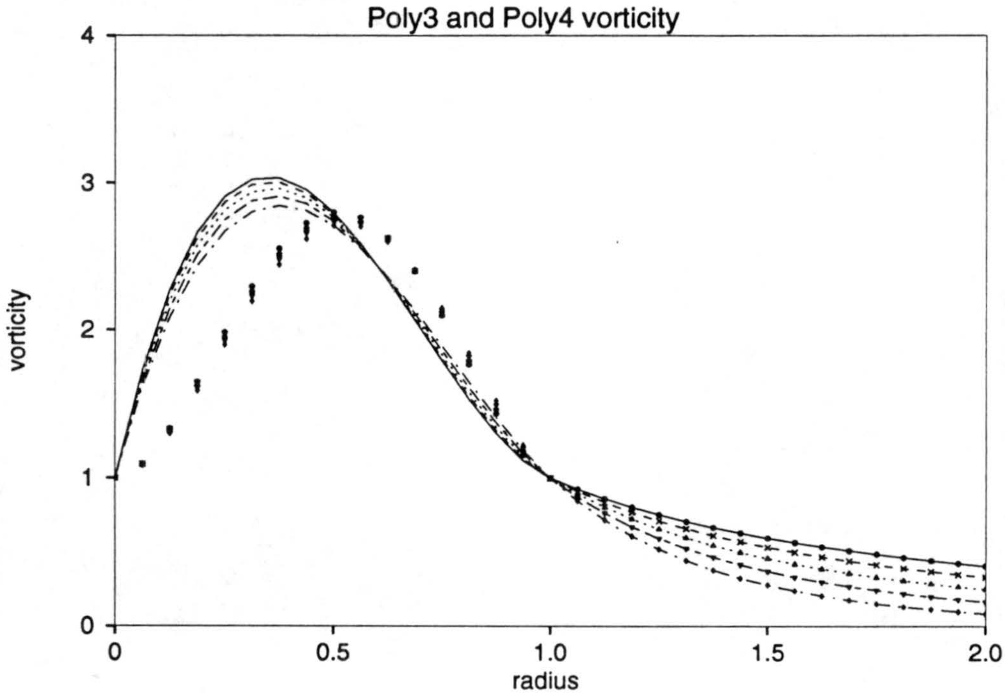

Figure B.4: Velocity (top) and vorticity (bottom) structure of the poly3 (lines) and poly4 (symbols) profiles for several values of p. Here $\zeta_0 = 1.0$.